Journal of
Clinical Medicine

MDPI

Review

Multimodality Cardiac Imaging in Cardiomyopathies: From Diagnosis to Prognosis

Guillem Casas [1,2,3,*] and José F. Rodríguez-Palomares [1,2,3,*]

[1] Cardiovascular Imaging Unit and Inherited Cardiovascular Diseases Unit, Cardiology Department, Hospital Universitari Vall d'Hebron, Vall d'Hebron Institut de Recerca, 08035 Barcelona, Spain
[2] Department de Medicina, Universitat Autónoma de Barcelona, 08035 Barcelona, Spain
[3] Centro de Investigación Biomédica en Red en Enfermedades Cardiovasculares, 28029 Madrid, Spain
* Correspondence: gcasas@vhebron.net (G.C.); jfrodriguez@vhebron.net (J.F.R.-P.)

Abstract: Cardiomyopathies are a group of structural and/or functional myocardial disorders which encompasses hypertrophic, dilated, arrhythmogenic, restrictive, and other cardiomyopathies. Multimodality cardiac imaging techniques are the cornerstone of cardiomyopathy diagnosis; transthoracic echocardiography should be the first-line imaging modality due to its availability, and diagnosis should be confirmed by cardiovascular magnetic resonance, which will provide more accurate morphologic and functional information, as well as extensive tissue characterization. Multimodality cardiac imaging techniques are also essential in assessing the prognosis of patients with cardiomyopathies; left ventricular ejection fraction and late gadolinium enhancement are two of the main variables used for risk stratification, and they are incorporated into clinical practice guidelines. Finally, periodic testing with cardiac imaging techniques should also be performed due to the evolving and progressive natural history of most cardiomyopathies.

Keywords: cardiomyopathy; multimodality cardiac imaging techniques; diagnosis; prognosis; left ventricular ejection fraction; late gadolinium enhancement

Citation: Casas, G.; Rodríguez-Palomares, J.F. Multimodality Cardiac Imaging in Cardiomyopathies: From Diagnosis to Prognosis. *J. Clin. Med.* **2022**, *11*, 578. https://doi.org/10.3390/jcm11030578

Academic Editor: Andrea Igoren Guaricci

Received: 8 December 2021
Accepted: 17 January 2022
Published: 24 January 2022

1. Introduction

Cardiomyopathies constitute a heterogeneous group of diseases that affect the muscle of the heart and present a very diverse etiology. Classically, the European Society of Cardiology (ESC) classifies these diseases as hypertrophic, dilated, arrhythmogenic, restrictive, or other cardiomyopathies [1]. Additionally, all of them are subclassified as familial/genetic or non-familial/non-genetic. Cardiomyopathies present variable expressions and symptoms that can change over time. Thus, periodic evaluation using cardiac imaging techniques is essential throughout follow-up. These techniques can help us to diagnose, guide treatment, and optimize patients' prognosis.

The patient evaluation includes anamnesis, physical examination, an electrocardiogram, and transthoracic echocardiography (TTE) that may raise suspicion of cardiomyopathy. This information is usually complemented with a cardiovascular magnetic resonance (CMR) that provides more precise anatomic and functional evaluation, as well as excellent tissue characterization with prognostic implications. Additionally, some patients may require a nuclear medicine test or cardiovascular computed tomography (CT).

In this manuscript, we will review the information that the different imaging techniques offer in the diagnosis and management of these patients.

2. Hypertrophic Cardiomyopathy

Hypertrophic cardiomyopathy (HCM) is defined by an increase in left ventricular (LV) wall thickness and/or LV mass, unexplained by LV loading conditions. HCM is the most prevalent cardiomyopathy, affecting approximately 1:500 of the adult population, and is usually caused by mutations in sarcomeric genes [2,3].

TTE is the first-line imaging modality for HCM evaluation: a maximal wall thickness >15 mm (or higher than two standard deviations from normal corrected for age, gender, and height) or asymmetric septal hypertrophy (septal/posterior wall thickness) ratio >1.3 (or >1.5 in hypertensive patients) is suggestive of HCM (Figure 1) [4]. A wall thickness ≥30 mm is associated with a higher risk of sudden cardiac death (SCD) [2,3].

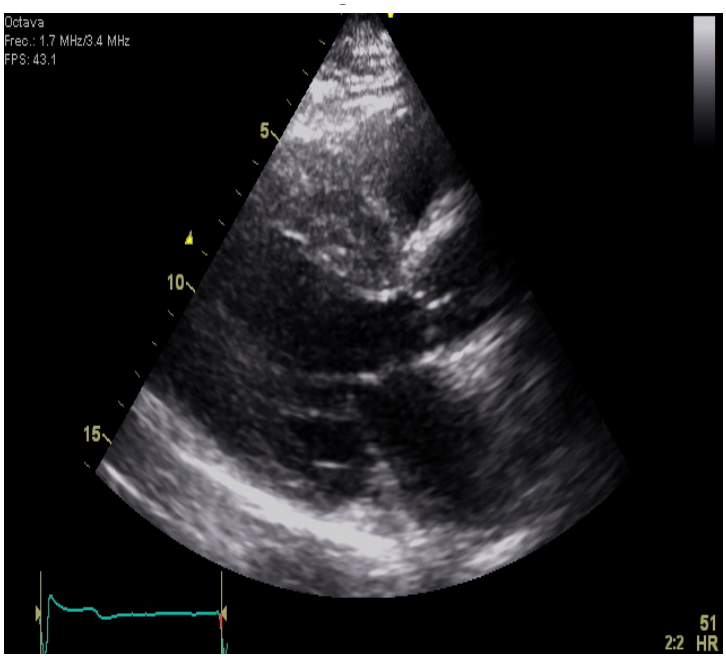

Figure 1. A parasternal long-axis view of a patient with septal HCM. Note the marked increase in septal wall thickness and the asymmetry compared to the posterior wall.

TTE allows for localization of the hypertrophy and hence identification of different phenotypes: septal, septal reverse, apical, or diffuse HCM, among others (Figure 2). In addition, patients with HCM present ancillary signs that, although non-specific, can help in the diagnosis: papillary muscle abnormalities (hypertrophic, bifid or trifid, and with an apical insertion), false tendons, myocardial clefts or crypts, aneurysms, or mitral valve and subvalvular structure abnormalities (elongated mitral leaflets with/without systolic anterior motion -SAM-) (Figure 3) [5].

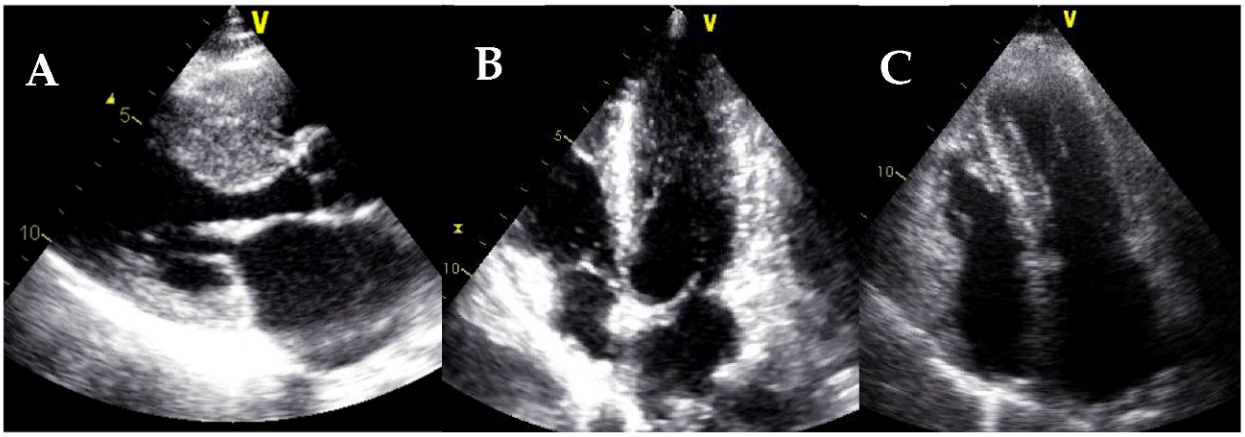

Figure 2. Different hypertrophic cardiomyopathy phenotypes. (**A**) Septal HCM. (**B**) Apical HCM. (**C**) Diffuse HCM.

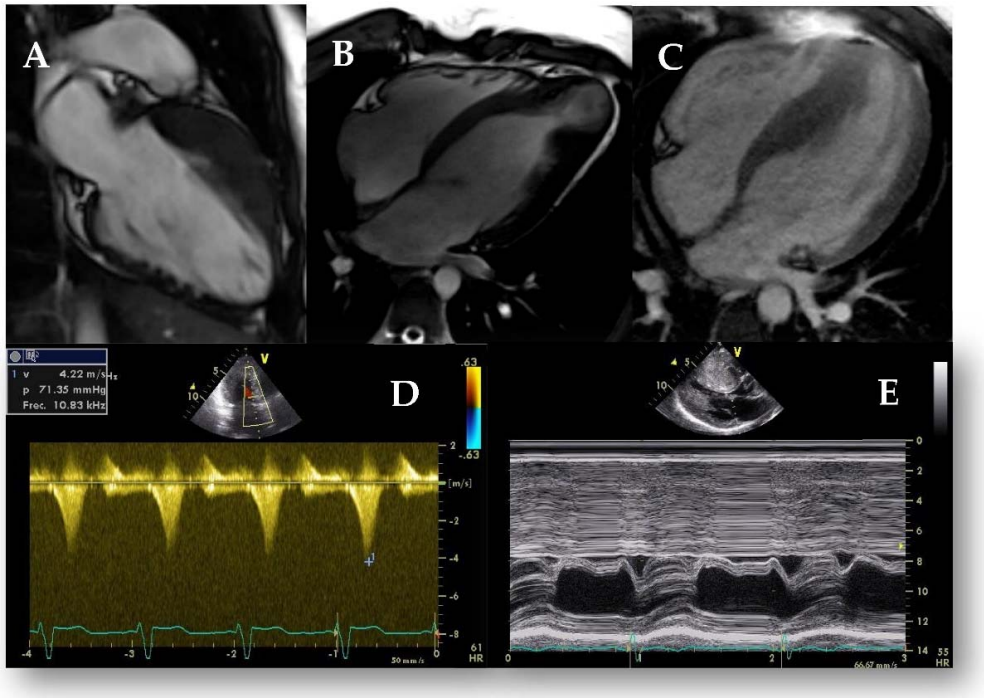

Figure 3. Ancillary signs in HCM. (**A**) Myocardial crypts in the inferior wall. (**B**) Apical aneurysm in a patient with apical HCM. (**C**) Apical insertion of the papillary muscles in a patient with septal HCM. (**D**) Outflow tract obstruction measured on Doppler CW, note the dagger-shaped curve. (**E**) SAM evidenced on M-mode: see the movement of the anterior mitral leaflet towards the septum in systole.

Moreover, the presence of LV outflow tract obstruction (LVOTO) can be easily evaluated and is defined as a peak gradient higher than 30 mm Hg at rest or after provocative maneuvers (typically observed as a dagger-shaped curve on continuous wave Doppler, Figure 3D). LVOTO differentiates between obstructive and non-obstructive HCM, with important therapeutic and prognostic implications [2,3]. Assessment of LV systolic function or LV ejection fraction (LVEF) is also important because it remains an important predictor of events [6]. Patients with an LVEF <50% present a poor prognosis [7] and should be considered for prophylactic implantable cardioverter-defibrillator (ICD) according to the recent American guidelines [3]. In addition, the anteroposterior left atrial diameter should be measured, and the diastolic function should be assessed. The maximal wall thickness, the left atrial diameter, and LVOTO have been incorporated into the risk prediction model of SCD [8] endorsed by the ESC [2].

Strain parameters from speckle-tracking TTE constitute markers of LV systolic function and are more sensitive than LVEF to systolic impairment. An abnormal global longitudinal strain (GLS) has been associated with worse outcomes in HCM [9], even though clear cut-off values are not available due to lack of standardization. Other techniques, such as circumferential strain or LV rotation and twist mechanics, are not routinely recommended.

CMR has become the gold standard technique for HCM evaluation and should be performed in all patients [4]. Beyond more accurate measurement of LV wall thickness and LVEF, CMR allows for tissue characterization with late gadolinium enhancement (LGE) sequences (Figure 4). Artificial intelligence and machine learning could further improve the accuracy of wall thickness measurements [10].

LGE is a frequent finding in HCM (about 60% of patients) [6,11–13], correlates with the presence of myocardial fibrosis [14], and usually affects the most hypertrophied segments with an intramural pattern. In addition, its location in areas of septal-free wall junctions is a common finding. The presence of LGE has been consistently associated with adverse outcomes and especially with SCD risk [11,15,16].

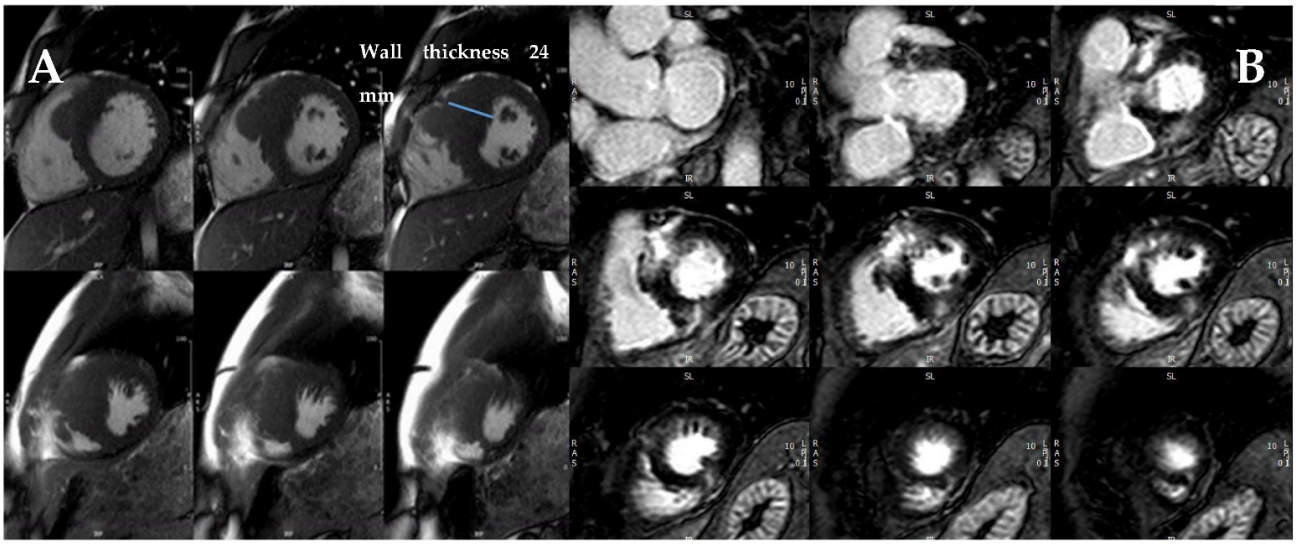

Figure 4. CMR study of a patient with septal HCM. (**A**) Maximal wall thickness measured on the short-axis cine stack at end-diastole. (**B**) Post-contrast T1 sequences showing extensive basal and mid-anteroseptal LGE with an intramyocardial pattern.

Quantification of LGE, usually as the percentage of total LV mass using the five standard deviation method [17], has emerged as a powerful predictor of SCD, both in obstructive and non-obstructive, low- and high-risk HCM [6,11–13,18] and with better predictive value than the ESC calculator [8]. An LGE >15% has been proposed as a risk marker for SCD [3,16,19]. Contrarily, outcomes of patients with a low LGE amount (<5%) are comparable to those without LGE [6,12]. Progression of LGE extension throughout follow-up has also been reported in HCM patients and has been related to adverse cardiac remodeling and worse prognosis [18]. Owing to the strong evidence, "extensive" LGE has been incorporated as a parameter for prophylactic ICD implantation in the recent American guidelines, which also recommend performing a CMR every 3–5 years to evaluate disease progression [3].

Emerging CMR sequences, such as T1 and T2 mapping and extracellular volume (ECV), allow for quantitative analysis of tissue characteristics and are more sensitive than LGE for the detection of myocardial fibrosis, especially in case of diffuse interstitial fibrosis (Figure 5) [20]. Further, T1 and T2 mapping are useful in the differential diagnosis of left ventricular hypertrophy [21]. Small studies have so far reported prognostic implications of T1 mapping [22] and ECV [23] values. However, further studies are needed to validate the prognostic implications of mapping sequences to fully incorporate them into daily clinical practice.

Stress echocardiography (SE) is another useful technique in the assessment of HCM because one-third of patients have latent LVOTO. SE is safe and usually performed in a semi-supine position, while the use of dobutamine is not recommended in HCM. LVOTO, LV systolic function (LVEF and GLS), LV diastolic function (E/E'), dynamic mitral regurgitation (usually secondary to SAM) and tricuspid regurgitation (TR) velocity should be evaluated at rest, at peak stress, and post-exercise (Figure 6) [24]. Exercise-induced significant LVOTO (>50 mmHg) is a marker of worse prognosis and can be used to guide treatment [2,3,24]. A diastolic stress test may also be performed; an increase in E/E' > 14 and peak TR velocity >2.8 m/s has been invasively correlated with elevated LV filling pressures during exercise [25] and is a marker of poor exercise tolerance [24]. The role of SE in the detection of inducible ischaemia in HCM is controversial. In this scenario, stress CMR with vasodilators is usually preferred, and signs of microvascular dysfunction may be observed [4].

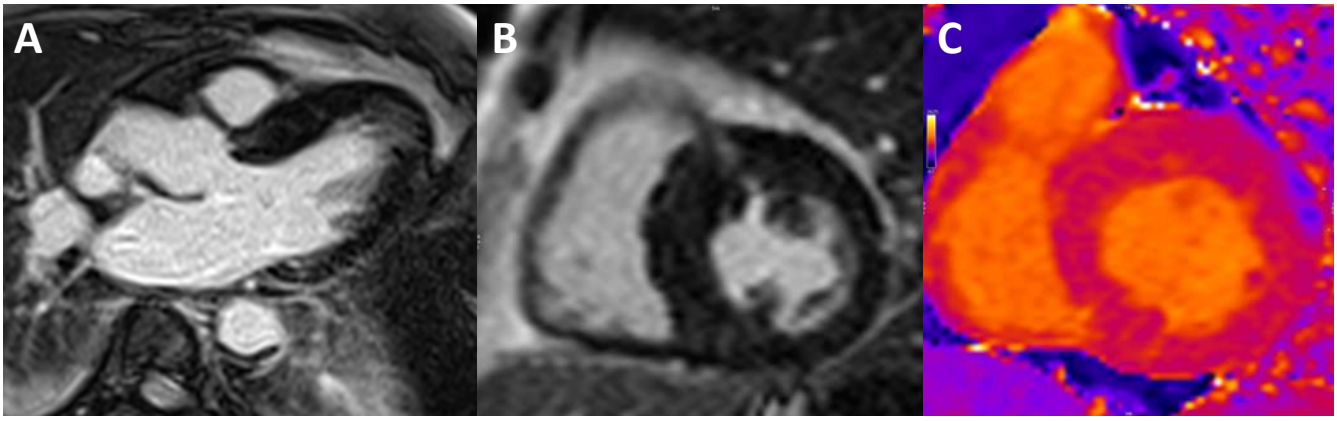

Figure 5. CMR study of a patient with septal HCM. (**A**,**B**) LGE sequences with heterogeneous contrast uptake in the basal and mid-anteroseptal segments. (**C**) Native T1 mapping sequence with an increased native T1 value of 1108 ms in the basal anteroseptal segment (reference range 950–1050 ms).

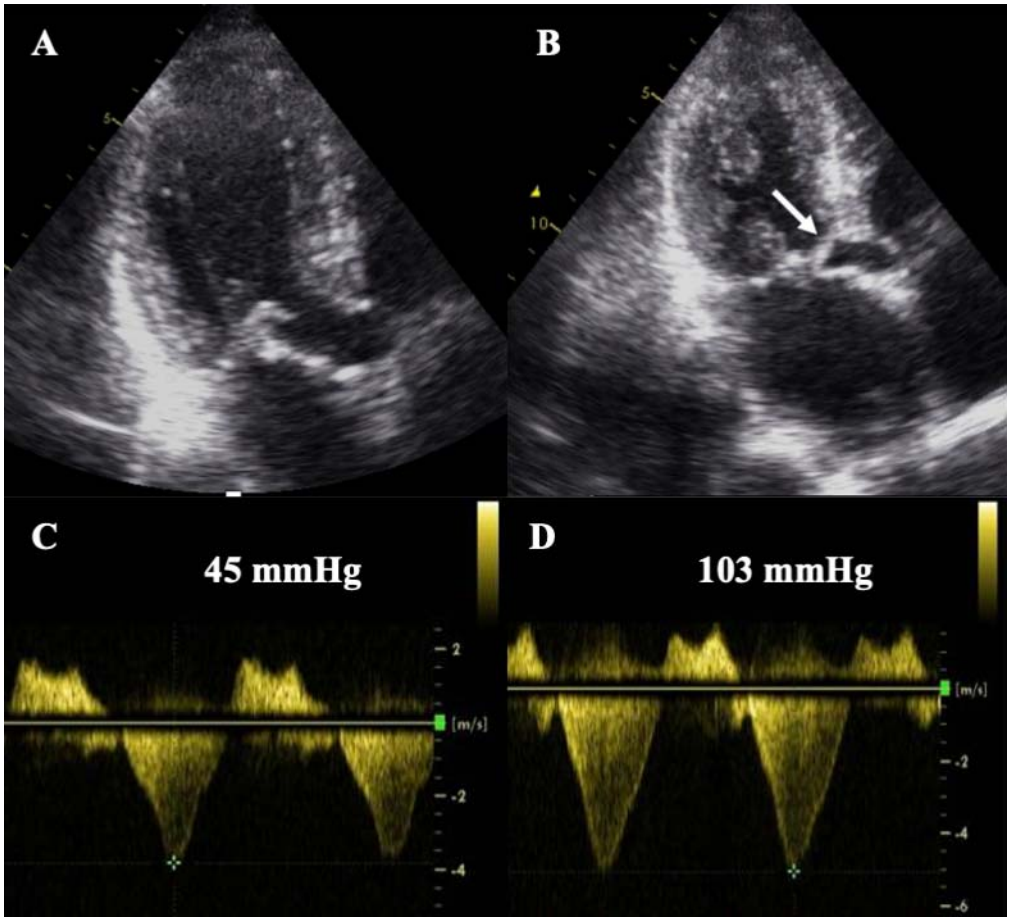

Figure 6. Stress echocardiography in a patient with HCM. Note the marked increase in SAM (**B**, white arrow) and the significant increase in LVOTO (**D**) at peak stress compared to the basal situation (**A**,**C**).

The role of cardiac CT in HCM is secondary and may be considered to exclude coronary artery disease. Recently, assessment of myocardial fibrosis by delayed enhanced CT has been described with an adequate agreement with LGE by CMR [26]. Even though data is still scarce, and no clinical implications should be attributed, it might become an alternative for those patients who have a contraindication for CMR.

Table 1 describes the main imaging diagnostic and prognostic findings in HCM.

Table 1. Summary of imaging findings in HCM.

Diagnostic Criteria	Ancillary Signs	Prognostic Markers
Maximal wall thickness >15 mm (>13 mm in relatives of HCM patients)	Papillary muscle abnormalities	Maximal wall thickness (>30 mm)
Asymmetric septal hypertrophy (ratio septal/posterior wall thickness >1.3 or >1.5 in hypertensive patients)	Mitral valve and subvalvular structure abnormalities	Left atrial size (anteroposterior diameter)
	Myocardial clefts/crypts	Maximum LVOT gradient (at rest or induced by exercise)
	Aneurysms	LVEF < 50%
		Abnormal GLS
		Presence, extension, and progression of LGE
		Increased T1/ECV values

3. Dilated Cardiomyopathy

Dilated cardiomyopathy (DCM) is defined by LV (or biventricular) systolic dysfunction (LVEF < 45%) and dilatation (LV end-diastolic volumes or diameters >2 standard deviations from normal corrected by age, gender, and body surface area) not attributed to loading conditions or coronary artery disease (Figure 7). DCM affects approximately 1:2500 adults, can be both genetic and acquired, and is a leading cause of heart failure [27].

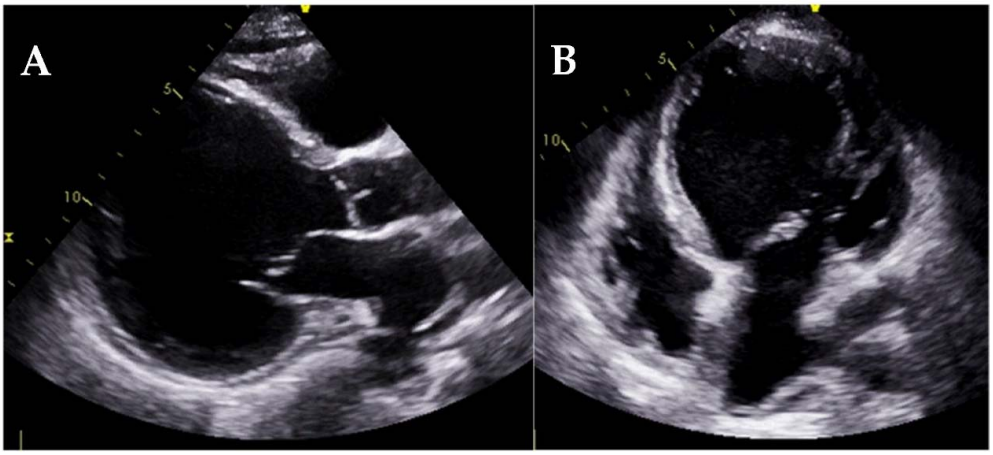

Figure 7. Transthoracic echocardiography of a patient with dilated cardiomyopathy, showing a parasternal long-axis view (**A**) and an apical 4-chambers view (**B**). Note the marked dilatation of the left ventricle and the spherical pattern.

TTE allows for both anatomical and functional assessment. Three-dimensional transthoracic echocardiography (3D TTE) is increasingly used due to improvements in technology and automated software and has the advantage of direct LV measurements with no geometric assumptions (Figure 8). Most importantly, 3D TTE is more accurate and reproducible than conventional two-dimensional (2D) TTE and shows better agreement with CMR values. However, 3D TTE depends on good image quality, requires more advanced technical skills, and normal values are less well established [28].

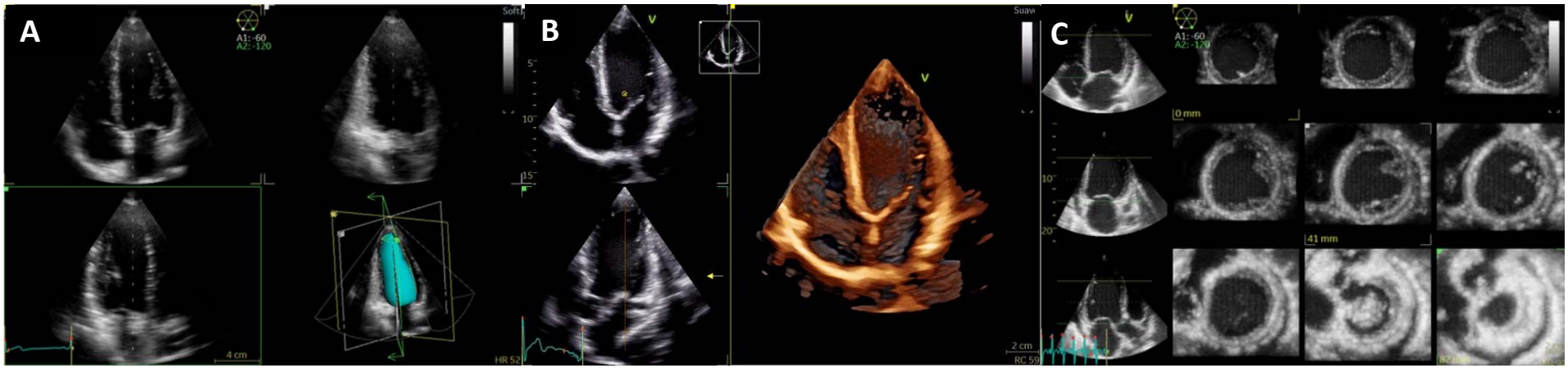

Figure 8. Three-dimensional transthoracic echocardiography of the left ventricle. (**A**) Triplane view of the LV allows simultaneous and single-beat acquisition of the three apical views. By tracing the endocardial borders, the LV volume is obtained (surface rendering, bottom right). (**B**) Real-time single-beat 3D acquisition of the LV from the apical window. Volume renders allow for offline reconstructions. (**C**) Tomographic multislice obtained from a multiple-beat apical view. Wall motion abnormalities can be assessed with this technique.

LVEF remains the strongest predictor of events in DCM; thus, patients with an LVEF ≤35% must be considered for optimal medical treatment and prophylactic ICD (with/without cardiac resynchronization therapy, CRT) [29,30]. However, an LVEF ≤35% has proven to have a low sensibility and specificity for SCD prediction, so additional predictors are required. Strain parameters, both GLS (Figure 9) and global circumferential strain (GCS) have been associated with cardiovascular events and present an incremental prognostic value over LVEF [31]. Myocardial work (MW) is a novel quantitative parameter that incorporates both strain and LV pressure variables (Figure 10) [32]. Initial reports suggest that not only MW is related to outcomes, but also has an additional prognostic role over both LVEF and GLS in DCM [33].

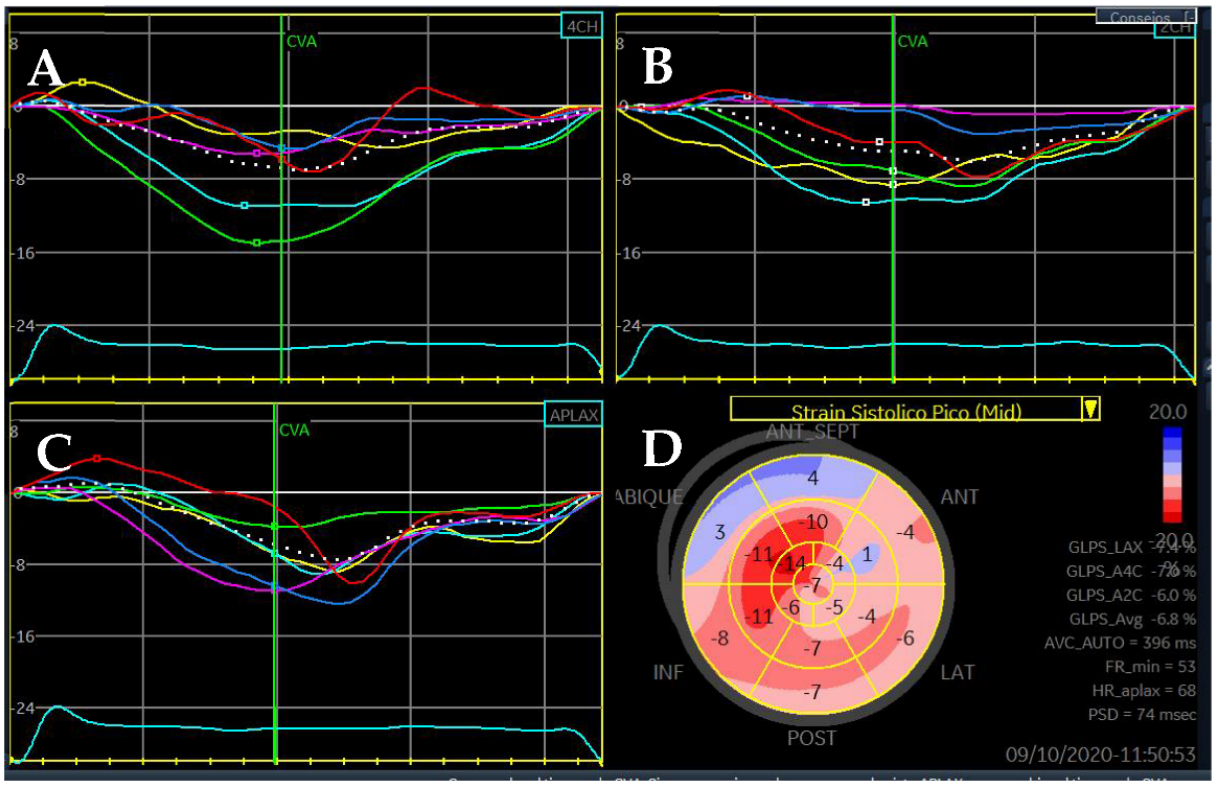

Figure 9. Longitudinal strain analysis of a patient with DCM: 4 chambers (**A**), 2 chambers (**B**), 3 chambers (**C**), and bull's eye plot (**D**). Note the diffusely affected longitudinal strain, consistent with depressed LVEF, and positive values in the basal septum suggestive of dyskinesia in these segments.

Stress echocardiography (SE) is also useful for risk stratification in DCM. Dobutamine is most often used, with either low or high-dose protocols (10 or 40 µg/kg/min), and the contractile response is assessed. An increase by ≥5% in LVEF at peak stress is defined as a contractile reserve and is associated with improved outcomes and reverse remodeling in DCM [24,34]. SE may also be used to exclude ischaemic etiology.

CMR should be performed at least once in all DCM patients since it is the gold standard technique for the assessment of biventricular volumes, systolic function, and tissue characterization. LGE is common in DCM and traduces myocardial fibrosis [35,36], usually with a septal mid-wall pattern (Figure 11). LGE has been consistently described as a strong and independent predictor of outcomes in DCM [35–37], and specifically for SCD [35,37,38]. The absence of LGE is also associated with reverse remodeling [37], which confers improved survival in DCM. Of note, LGE shows incremental prognostic value over LVEF [39], even in patients with only mild or moderate systolic dysfunction [40].

The extension, localization, and pattern of LGE have also been associated with prognosis [41,42]; a higher burden of LGE, septal LGE, and multiple patterns (combined septal

and free-wall, epicardial, and transmural LGE) are related to higher mortality or SCD. The risk of adverse outcomes is also higher in patients with progression of LGE over time [43]. Considering the important prognostic role of LGE and the aforementioned limitations of LVEF, a combined algorithm has recently been proposed to enhance the identification of patients at high risk for SCD who should be considered for prophylactic ICD [42]. However, clinical guidelines are only based on LVEF [29,30].

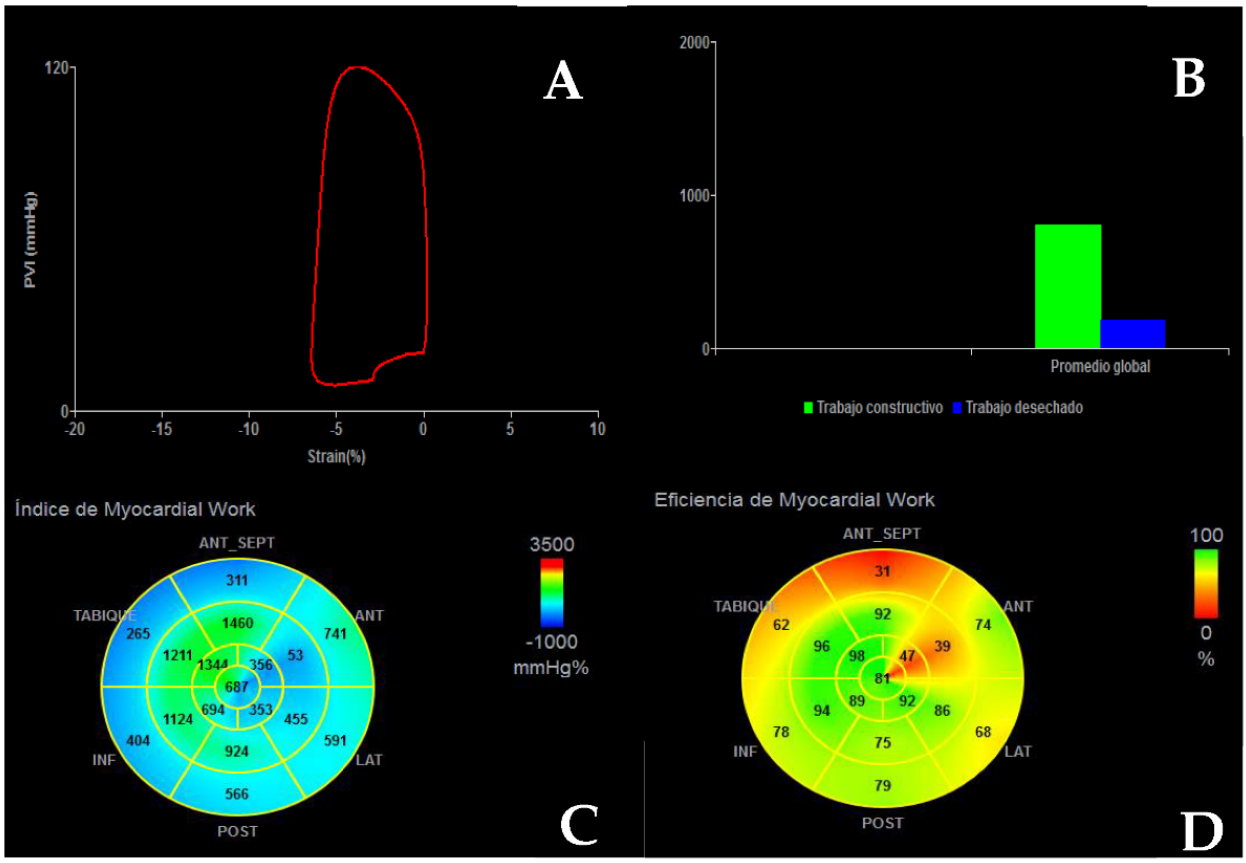

Figure 10. Myocardial work analysis in a patient with DCM. (**A**) Strain—pressure loop. (**B**) Comparison of constructive work (green) and wasted work (blue). (**C**) Bull's eye plot of myocardial work index (mmHg%). (**D**) Bull's eye plot of myocardial work efficiency (%).

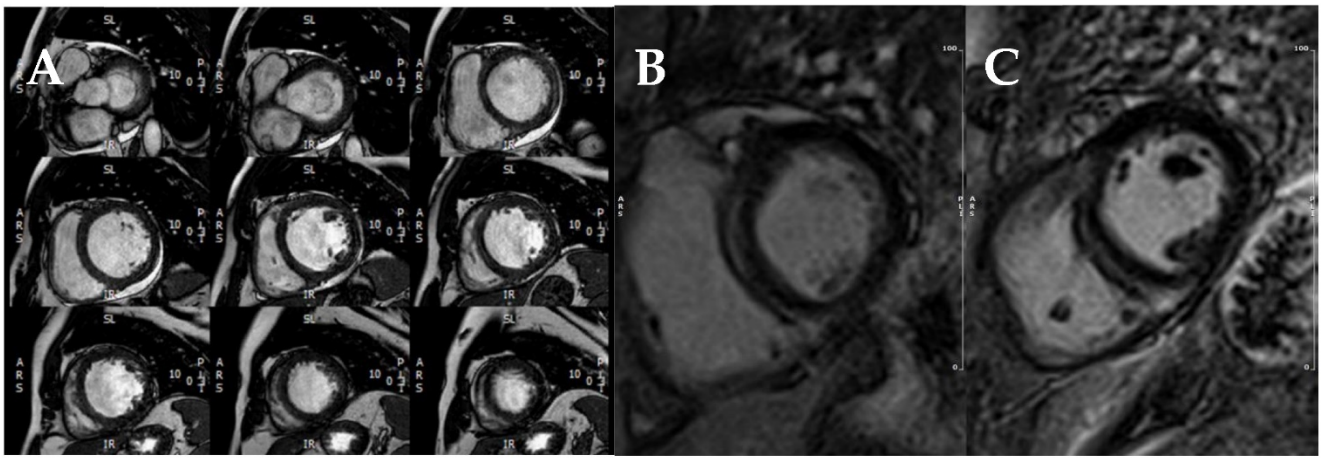

Figure 11. CMR study of a patient with DCM. (**A**) Short-axis cine stack. (**B**,**C**) Post-contrast T1 sequences showing a typical LGE pattern with a lineal mid-septum uptake as well as a focal uptake in the septum-free wall inferior junction.

GLS by CMR (Figure 12) has been shown to be associated with outcomes in DCM, and most importantly to improve risk classification beyond LVEF and LGE [44]. However, it has not been standardized and no cut-off points have been proposed, so routine clinical use is not yet recommended. Mapping techniques have also been evaluated in DCM; higher T1 and ECV values have been shown to have prognostic implications irrespective of LVEF and LGE [45]. Furthermore, an increased native T2 value indicates the presence of myocardial edema, which could suggest the presence of inflammatory cardiomyopathy [46]. These techniques offer promising new tools for risk stratification, but further validation is still required.

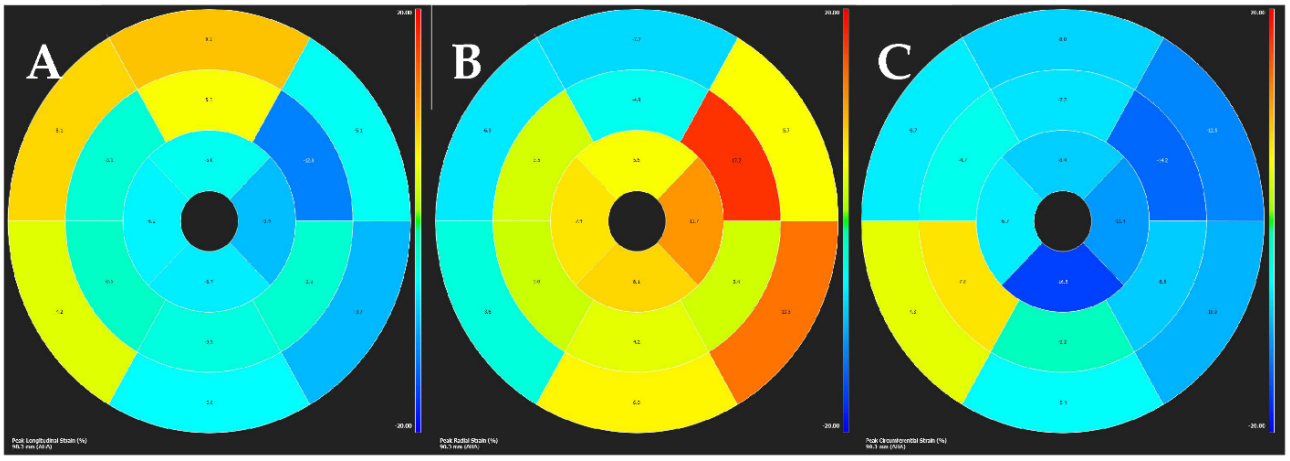

Figure 12. Strain analysis by CMR obtained with feature-tracking software in a patient with DCM. Endocardial and epicardial segmentation of short and long-axis is required, both at end-diastole and end-systole. Thus, longitudinal (**A**), radial (**B**), and circumferential (**C**) strain are simultaneously acquired.

Assessment of right ventricle (RV) size and systolic function is recommended in all patients since RV systolic dysfunction is a common finding and an independent predictor of poor outcome [47]. Different techniques may be applied: fractional area change [48], peak longitudinal strain of RV free wall [49] by TTE, or RV ejection fraction (RVEF) by CMR [47]. The same advantages and limitations previously mentioned in 3D TTE also apply to the RV; specifically, global chamber including RV inflow and outflow tracts and apical regions can only be assessed by 3D TTE and not 2D TTE (Figure 13) [28]. Secondary (functional) mitral regurgitation and diastolic dysfunction should also be evaluated since they are associated

with cardiovascular events [50]. LV GLS [51], left atrial strain [52] and MW [53,54] by TTE, as well as septal viability on CMR [54], have been identified as predictors of response to CRT.

Other imaging modalities are rarely used in DCM. Nuclear imaging can analyze cardiac sympathetic innervation, which has been associated with ventricular arrhythmias and adverse prognosis [55]. Cardiac CT is commonly used to exclude coronary artery disease. Recent studies have shown the ability of delayed enhancement CT to detect myocardial fibrosis, with comparable performance to LGE by CMR [56]. However, results are still preliminary, and no clinical studies are available, so routine use is not recommended.

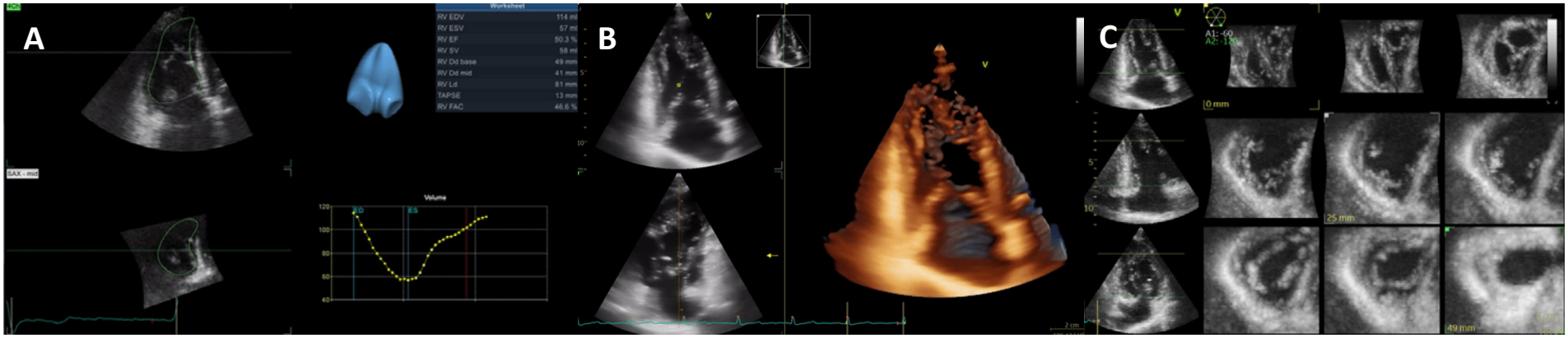

Figure 13. Three-dimensional transthoracic echocardiography of the right ventricle. (**A**) By tracing the endocardial RV borders (top and bottom left), a 3D volume of the RV (top right) is obtained throughout the cardiac cycle (bottom right) and 3D RVEF is calculated. Note the RV inflow and outflow tract in the 3D model. (**B**) Real-time single-beat 3D acquisition of the RV from the dedicated apical window. (**C**) Tomographic multislice obtained from a multiple-beat apical view.

Table 2 describes the main imaging prognostic findings in DCM.

Table 2. Summary of prognostic imaging markers in DCM.

LVEF $\leq$ 35%
RV systolic dysfunction (RVEF < 45%)
Significant (secondary) mitral regurgitation
Advanced diastolic dysfunction
Abnormal strain and myocardial work values
Presence, extension, pattern, and progression of LGE
Increased T1 and ECV values

4. Restrictive Cardiomyopathies

Restrictive cardiomyopathies (RCM) account for less than 5% of all cardiomyopathies and have a highly varied etiology (Table 3).

Table 3. Classification of restrictive cardiomyopathies.

Restrictive Cardiomyopathy			
Non-Infiltrative Disorders	**Infiltrative Disorders**	**Storage Diseases**	**Endomyocardial Diseases**
• Idiopathic • Hereditary (sarcomere mutations . . .) • Systemic sclerosis	• Amyloidosis • Sarcoidosis • Hereditary hyperoxaluria	• Anderson–Fabry disease • Danon disease • Pompe disease • Gaucher disease • Iron overload • Hereditary hemochromatosis	• Carcinoid • Endomyocardial fibrosis • Endocardial fibroelastosis • Metastatic tumor • Chemotherapy • Radiation therapy

RCM is characterized by a marked alteration of myocardial compliance: severe diastolic dysfunction and a preserved systolic function (at least in early stages). The initial diagnosis is performed by TTE showing a normal/increased LV wall thickness (generally with a concentric/symmetric distribution), a restrictive pattern by Doppler, absence of left ventricular dilatation, preserved LVEF, and a marked biatrial dilatation [57]. However, although TTE is crucial for the initial approach and raising diagnostic suspicions, its role is limited when establishing the differential diagnosis, in which case CMR is highly relevant.

4.1. Idiopathic Restrictive Cardiomyopathy

Idiopathic restrictive cardiomyopathy is a very uncommon disease affecting predominantly children and young adults with a familial pattern. It is characterized by the presence of a restrictive diastolic filling pattern (increased left ventricular end-diastolic pressure), normal left ventricular dimensions, absence of an increased left ventricular mass, normal left and right ventricular function, and absence of any other cardiac or pericardial diseases [58].

4.2. Cardiac Amyloidosis

Cardiac amyloidosis (CA) is an infiltrative disease caused by an extracellular accumulation of amyloid fibers. Most patients are affected by light chains (primary or AL amyloidosis) or by transthyretin (ATTR amyloidosis), either the hereditary form (ATTRm) or the wild type (ATTRwt) [59].

Among the main TTE findings, the following "red flags" should raise suspicion of CA [60]: left ventricular wall thickness > 12 mm, myocardial sparkling (Figure 14), increased valvular thickness, thick interatrial septum, low stroke volume, paradoxical low-flow low-gradient aortic stenosis, restrictive filling pattern by Doppler, and apical sparing pattern on strain analysis (a reduced global longitudinal strain with an apical to basal deformation ratio >2.1) (Figure 14), abnormal left atrial strain and pleural or pericardial effusion.

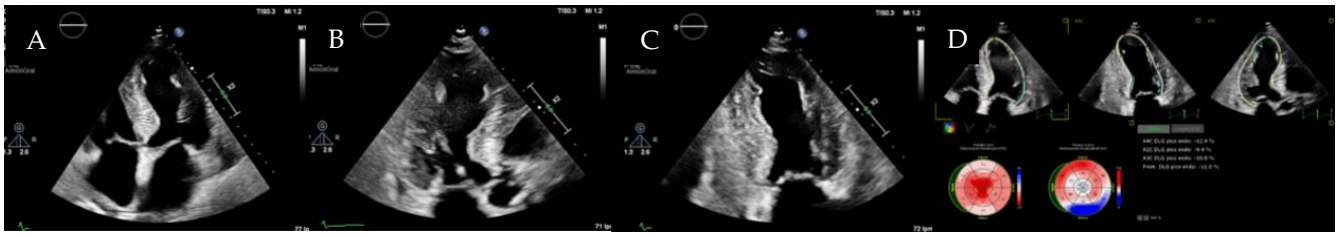

Figure 14. Apical 4-chamber (**A**), 3-chamber (**B**), and 2-chamber (**C**) views in a patient with cardiac amyloidosis (left ventricular wall thickness and sparkling). On the bull's eye strain images (**D**), the apical sparing pattern is displayed (right image).

The presence of a reduced GLS presents prognostic implications; a GLS >−14.8% has been associated with an increase in global mortality [61]. Although the apical sparing pattern is quite suggestive of CA, this pattern may not be present in patients with concomitant significant aortic stenosis [62].

CMR provides high-resolution structural and functional information, allows tissue characterization [60], and permits diagnosis at early stages compared to TTE [63]. The main findings, in addition to those described by TTE, are the difficulty to null the myocardial signal in LGE sequences, a global or diffuse LGE, and a marked increase in native T1 and ECV values (>40%) (Figure 15) [60,63,64].

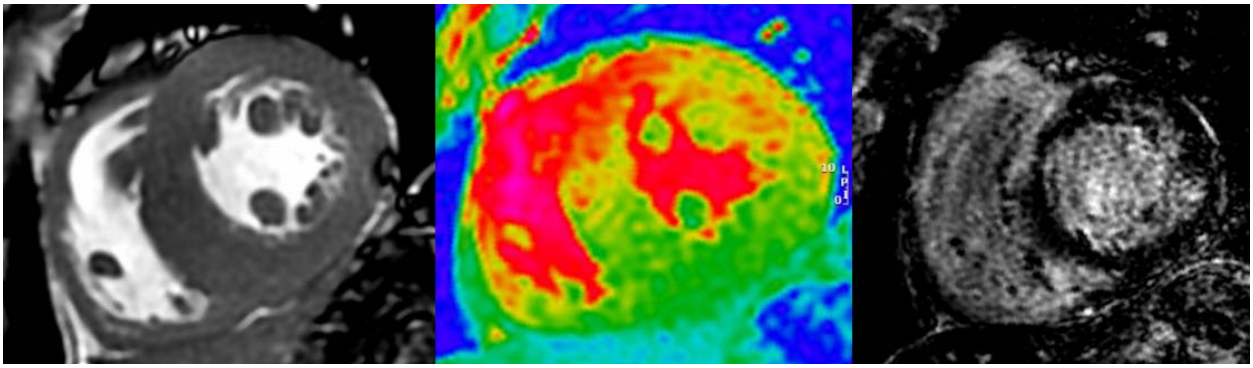

Figure 15. CMR findings in a patient with CA: left ventricular concentric hypertrophy (left), increased native T1 mapping values (red color in the central image), and diffuse LGE (right image).

As the disease progresses, there is an increase in LGE uptake, which is initially subendocardial and progressively becomes transmural (which is associated with an increase in overall mortality regardless of the type of amyloidosis) [65]. Additionally, a recent meta-analysis showed that ECV is the strongest diagnostic and prognostic imaging biomarker in CA [66], and an ECV >58% is associated with increased mortality in ATTR [67]. CMR cannot distinguish ATTR and AL forms, but there are characteristically-associated signs (Table 4) [64,65,67,68].

Either 99m technetium diphosphonate (Tc-DPD) or pyrophosphate (Tc-PYP) scintigraphy play a relevant role in diagnosing ATTR amyloidosis and allow early detection of cardiac involvement before TTE and CMR, however, false positives can be present [69]. Results are evaluated based on the Perugini scale: a grade 2 or 3 uptake (cardiac uptake similar to or greater than the ribs with/without a reduction in the bone uptake) has a positive predictive value around 100% [70]. Another means of quantification is the assessment of cardiac uptake compared to the contralateral chest (C/CL): a ratio $\geq$1.5 suggests the diagnosis of ATTR [68,70]. Prognostic implications of scintigraphy are still limited, however, a C/CL uptake >1.6 [71] or an apical sparing pattern [72] are associated with lower survival.

Table 4. Main differences between ATTR and AL amyloidosis.

	ATTR	AL
Left ventricular wall thickness and LV mass	++++	++
Asymmetrical septal hypertrophy	79%	14%
Transmural LGE	63%	27%
Subendocardial LGE	24%	39%
Native T1 elevation	++	++++
Native T2 relaxation time	++	++++
ECV	++++	++

++ Mildly abnormal. ++++ Severely abnormal.

Table 5 describes the main imaging findings that should raise suspicion of cardiac amyloidosis.

Table 5. Main imaging red flags in cardiac amyloidosis.

Echocardiography	CMR	Scintigraphy
• Left ventricular wall thickness > 12 mm. • Myocardial sparkling • Pleural/pericardial effusion • Increased valvular thickness • Thick interatrial septum. • Low stroke volume. • Paradoxical low-flow low-gradient aortic stenosis. • Restrictive filling pattern. • Apical sparing pattern. • Abnormal left atrial strain.	• Increased LV wall thickness. • Increased myocardial LV mass • Bi-auricular enlargement • Difficulty to null the myocardial signal • Global or diffuse LGE, • Marked increase in native T1 values • Elevated extracellular volume (> 40%) • Presence of pleural or pericardial effusion	• Grade 2 or 3 uptakes in the Perugini scale. • C/CL uptake ≥ 1.5

4.3. Fabry Disease

Anderson–Fabry disease (FD) is a rare (approximate incidence 1:40,000) genetic lysosomal storage disorder caused by a mutation in the alpha-galactosidase A (GLA) gene with an X-linked inheritance.

The presence of concentric left-ventricular hypertrophy (LVH) is the most common finding in FD, however, other patterns have also been described: septal, asymmetric, or apical [73]. LVH is higher in men than in women, and it tends to appear at younger ages. Another common finding is the presence of a binary septum: a hyperechoic endocardium adjacent to a hypoechoic subendocardium (Figure 16A). Prominent papillary muscles have also been described, as well as RV hypertrophy. There is also dilation and left atrial dysfunction (systolic and early diastolic strain) that is associated with a higher incidence of supraventricular arrhythmias. Mitral and aortic valvular thickening are also frequent.

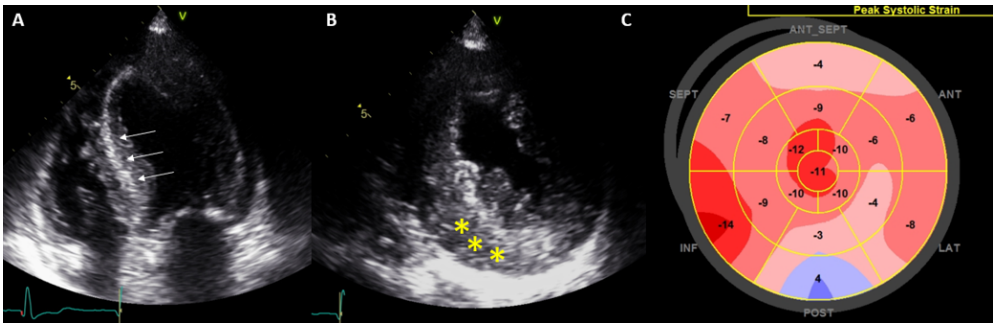

Figure 16. Echocardiographic signs in Fabry disease. (**A**) Binary septum (arrows), (**B**) concentric hypertrophy, and inferolateral fibrosis (*), (**C**) abnormal longitudinal strain more pronounced in the inferolateral wall (blue area) correlated with the fibrosis.

Generally, the biventricular systolic function is preserved until advanced stages of the disease, at least in terms of LVEF. However, FD patients show reduced values of GLS

and GCS compared to controls, which are more reduced in those with inferolateral LGE (Figure 16C); thus, an inferolateral longitudinal strain peak value <−12.5% suggests the presence of fibrosis with a sensitivity of 90% and a specificity of 97% [74].

Table 6 describes the main imaging findings in Fabry disease.

Table 6. Main echocardiographic findings in Fabry disease.

CARDIAC STRUCTURE	FINDINGS
Left ventricle	Concentric left ventricular hypertrophy Binary septum (low sensitivity and specificity for FD) Prominent papillary muscles Preserved LV function until end-stages Diastolic dysfunction Abnormal global longitudinal or radial strain, even in the absence of LVH
Right ventricle	Right ventricular hypertrophy Preserved RV function until end-stages Abnormal global longitudinal strain even with preserved EF
Atrium	Biauricular dilation Increased end-diastolic pressure Reduced auricular strain
Valves	Increase in mitral and aortic valve thickness Valvular regurgitation (generally, mild)
Aorta	Dilation of the aortic root and the ascending aorta (not descending aorta)

The most common finding in CMR is also the presence of concentric LVH. The typical LGE pattern is an intramyocardial uptake at the basal LV inferolateral wall, which is present in up to 50% of patients [75], and may progress to transmural extension together with a marked thinning of the myocardial wall (Figure 17).

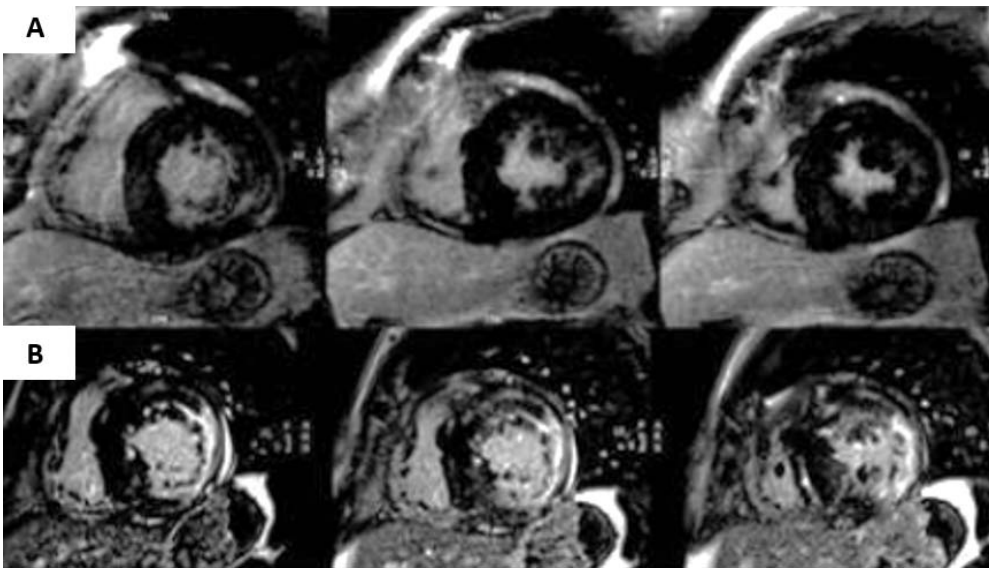

Figure 17. Late gadolinium enhancement pattern in a patient with Fabry disease. (**A**) Presence of LGE in the inferolateral wall. (**B**) Evolution of the same patient 5 years later, the presence of a thinning of the wall, a more extensive and transmural LGE pattern is observed.

The presence of LGE is indicative of irreversible myocardial damage; tfhus, clinical practice guidelines recommend starting treatment with a class I indication when there is

no or minimal fibrosis [76]. The presence of LGE is associated with a poorer response to medical treatment and an increased risk of cardiovascular events including SCD [74]. For this reason, some authors have suggested an ICD implantation in patients with a significant LGE mass; however, there are no available guidelines.

T1 and T2 mapping techniques may identify the presence of early myocardial damage before the onset of myocardial fibrosis. Given that the degree of myocardial infiltration is diffuse, it is recommended to assess the value of native T1 in all myocardial segments (Figure 18) [77]. Native T1 time has been inversely correlated with wall thickness, so that, the more hypertrophy the lower T1. Additionally, patients with ECG abnormalities present shorter T1 [77]. In the early stages, ECV is normal, suggesting that LVH is due to myocyte hypertrophy and not to extracellular fibrosis.

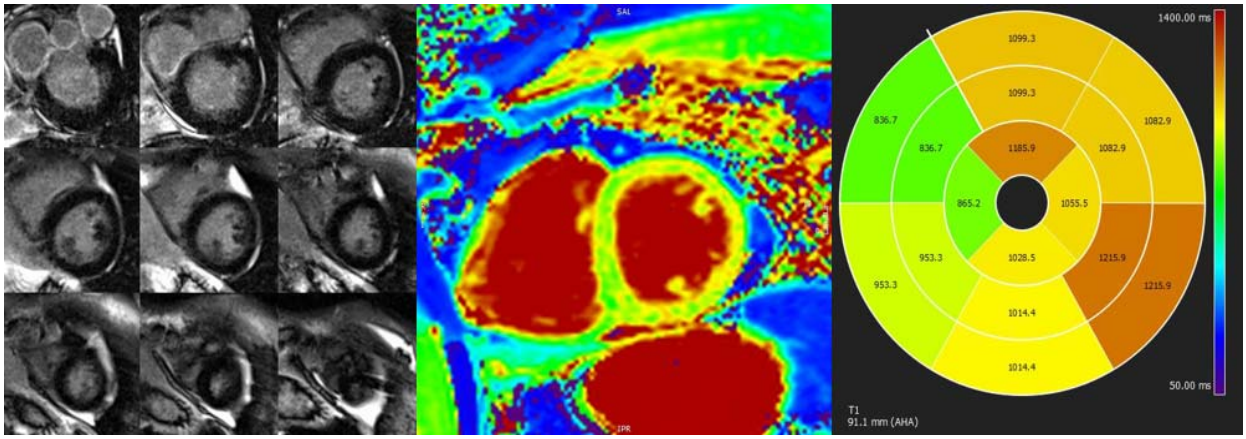

Figure 18. CMR findings in a patient with Fabry disease: (Left panel) presence of concentric left ventricular hypertrophy with no LGE. (Central panel) T1 mapping image of the same patient. (Right panel) bull's eye representation of the T1 mapping showing a short native T1 in the septum (glycosphingolipid accumulation) and a long T1 value in the inferolateral wall (diffuse fibrosis). T1 mapping abnormalities appear earlier than LGE.

FD must also be considered a chronic inflammatory disease. Thus, unlike patients with HCM, the presence of high native T2 values suggest FD, initially affecting the inferolateral wall and becoming progressively diffuse. Using 18F-fluorodeoxyglucose positron emission tomography (PET), an increase in the uptake of the tracer has also been described, confirming the presence of myocardial inflammation [78]. Finally, patients with FD also present a reduction in sympathetic activity, and 123I-meta-iodobenzylguanidine (MIBG) scintigraphy studies can differentiate stages of the disease [79]. The absence of myocardial denervation could play a relevant role in assessing the risk of developing ventricular arrhythmias and SCD.

4.4. Iron Overload Cardiomyopathy

Iron overload cardiomyopathy (IOC) is a secondary form of cardiomyopathy resulting from iron accumulation in the myocardium mainly because of genetically-determined iron metabolism disorders or multiple transfusions [80]. It has been described as a dilated cardiomyopathy, characterized by LV remodeling with chamber dilatation and reduced LVEF. However, primary hemochromatosis, a genetically determined condition leading to iron overload, is classically categorized as an infiltrative cause of restrictive cardiomyopathy. Moreover, secondary hemochromatosis may lead to severe diastolic LV dysfunction in the early stages of the disease, before LVEF is affected [80].

IOC can be very difficult to diagnose by TTE, therefore, CMR T2* imaging is considered the reference standard for detecting and quantifying myocardial iron overload. Abnormalities in CMR T2* can occur before the development of systolic or diastolic dysfunction and may be used to guide iron chelation therapy to prevent heart failure or death [81].

For easy classification into different IOC risk groups, the following classification has been adopted using a 1.5 Tesla MR scanner: patients with T2* >20 ms are regarded as not having cardiac iron overload, between 10–20 ms have mild to moderate cardiac iron load and those <10 ms are considered to have a heavy cardiac iron load [82].

4.5. Cardiac Sarcoidosis

Sarcoidosis is an inflammatory granulomatous disease that can involve any organ, with cardiac involvement (cardiac sarcoidosis, CS) in a quarter of patients. Clinical manifestations include heart block, atrial and ventricular arrhythmias, and heart failure. Diagnosis can be challenging but with the increased availability of advanced cardiac imaging, more cases are being identified.

TTE has limited sensitivity and specificity for the diagnosis of CS, however, it is often the initial imaging study. The TTE main findings include ventricular hypertrophy, diastolic dysfunction/restrictive filling pattern, wall motion abnormalities with a non-coronary distribution, aneurysms, and LV or RV systolic dysfunction [83]. CS patients who need pacing and have an LVEF <50% should be considered for CRT with ICD according to the recent ESC guidelines [84].

CMR plays an important role in the diagnosis and risk stratification of patients with CS. Although the presence of LGE may be non-specific, the subepicardial location, multifocal distribution, high signal intensity, and contiguous extension from the left to the right ventricle may increase the specificity of this finding for the diagnosis of CS [85]. Many studies have also demonstrated its prognostic value; LGE is associated with an increased risk of ventricular arrhythmias and all-cause mortality [85].

Cardiac PET using 18F-FDG has emerged as a cornerstone in the clinical diagnosis, prognostic evaluation, and monitoring of therapy in CS. FDG-PET/CT has a fair diagnostic accuracy for CS [86]. The classic pattern is one of 'perfusion–metabolism' mismatch, in which areas of 18F-FDG uptake correspond to areas of reduced or absent perfusion. FDG-PET/CT has a fair diagnostic accuracy for CS with a sensitivity of 89% and specificity of 78% [86]. An abnormal FDG uptake is associated with increased rates of ventricular arrhythmias and death, especially when located in the right ventricle [87] (Figure 19). Serial PET imaging is useful in monitoring disease activity and response to immunosuppressive therapy. Additionally, hybrid CMR-PET imaging has shown incremental value in determining disease activity and pattern [88].

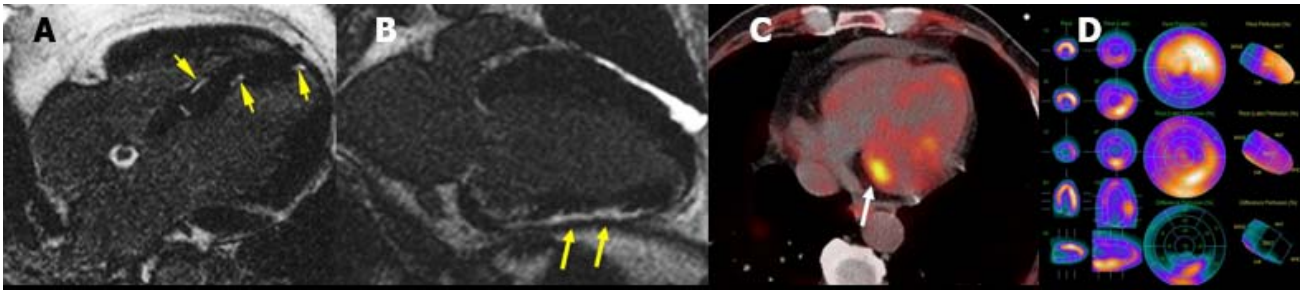

Figure 19. (**A**) Patchy LGE distribution in the septum (arrows) and (**B**) subepicardial LGE (arrows) in a patient with sarcoidosis. (**C**) 18F-FDG uptake in a patient with sarcoidosis (arrow). (**D**) Perfusion-metabolism mismatch in a patient with sarcoidosis (perfusion defect in the upper image, metabolism uptake in the mid image, and mismatch in the lower image).

4.6. Endomyocardial Fibrosis

Endomyocardial fibrosis (EMF) is a rare form of RCM characterized by an abnormal thickening of the endocardium due to fibrous tissue deposit [89] secondary to infections (typically in the tropical regions), inflammation, or toxic agents among others. Echocardiographic findings include apical obliteration due to endocardial thickening, a small ventricular cavity, and a marked restrictive diastolic pattern. EMF may affect primar-

ily the left ventricle, both left and right ventricles (in approximately half of the cases), or predominantly the right ventricle [90]. Apical thrombus is also a common finding and echocardiographic contrast may be used to differentiate them from the thickened myocardium (Figure 20).

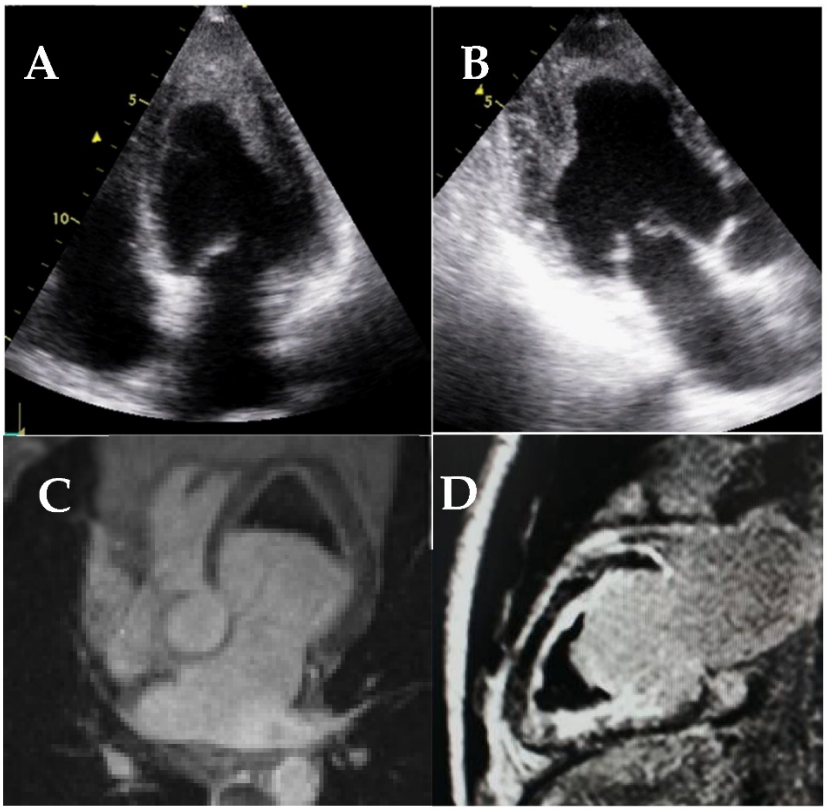

Figure 20. Transthoracic echocardiography (**A**,**B**) and cardiac magnetic resonance (**C**,**D**) of patients with endomyocardial fibrosis. Note the marked endocardial thickening of the mid and apical segments and apical obliteration of the left ventricle (**A**,**B**), the apical thrombus (**C**,**D**), and the endomyocardial fibrosis on LGE sequences (**D**).

CMR is the gold standard for EMF evaluation and specifically for localization, characterization, and quantification of fibrous tissue by LGE sequences. LGE strongly correlates with histopathological findings and its extension is associated with increased mortality risk [91]. CMR may also identify apical thrombus or calcifications.

5. Arrhythmogenic Cardiomyopathy

Arrhythmogenic cardiomyopathy (ACM) is an inherited heart muscle disorder predisposing to SCD, particularly in young patients and athletes. It is a cell-to-cell junction cardiomyopathy, typically caused by genetically-determined abnormalities of cardiac desmosomes. Pathological features include loss of myocytes and fibrofatty replacement of right or left ventricular myocardium. ACM diagnosis does not rely on a single gold standard test but is classically achieved using a scoring system, which encompasses familial and genetic factors, ECG abnormalities, arrhythmias, and structural/functional ventricular alterations [92]. The score was recently updated and simplified [93].

TTE is the initial diagnostic approach in ACM patients. A thorough RV assessment with dedicated RV planes is recommended if clinical suspicion is high (Figure 21). The presence of regional RV akinesia, dyskinesia, or aneurysms and either RV dilatation or RV systolic dysfunction are considered diagnostic criteria on the 2010 Task Force Criteria, with different cut-off points for TTE and CMR major or minor criteria (Table 7) [92]. These were

changed slightly in the Padua criteria [93], where RV dilatation and systolic dysfunction were defined according to nomograms, with no specific cut-off points.

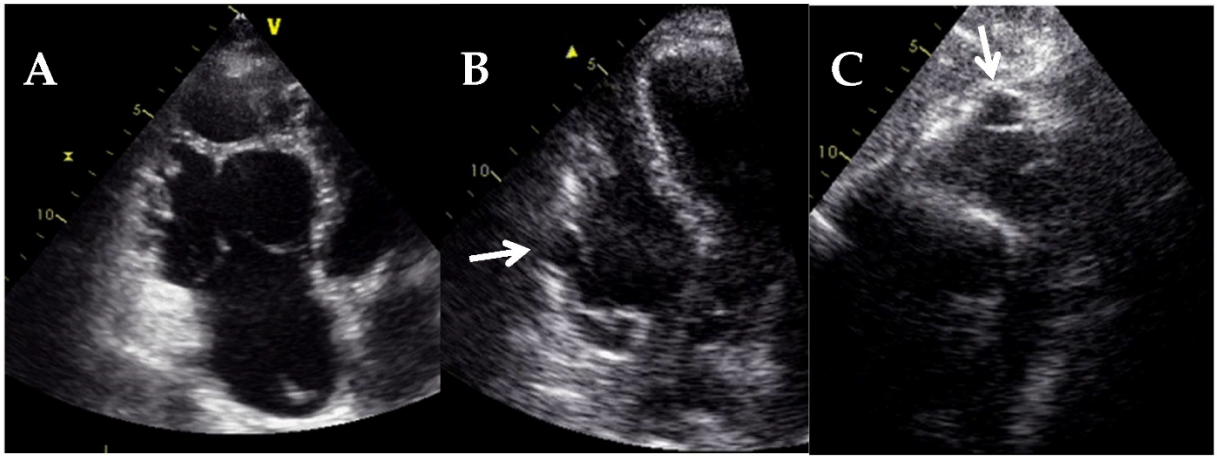

Figure 21. Transthoracic echocardiography of a patient with right ventricular arrhythmogenic cardiomyopathy. (**A**) RV dedicated apical 4-chamber view shows severe dilatation of the RV. RV dedicated apical 4-chamber view (**B**) and subcostal view (**C**) show the presence of aneurysms in the RV free wall (arrow).

Table 7. 2010 Task Force Criteria for the Diagnosis of Arrhythmogenic Right Ventricular Cardiomyopathy. Adapted from [92].

	Global and/or Regional Dysfunction and Structural Alterations
Major	By 2D TTE: regional RV akinesia, dyskinesia, or aneurysm and 1 of the following (end diastole): • PLAX RVOT $\geq$ 32 mm (corrected for body size [PLAX/BSA] $\geq$ 19 mm/m^2) • PSAX RVOT$\geq$ 36 mm (corrected for body size [PSAX/BSA] $\geq$ 21 mm/m^2) • Or fractional area change $\leq$ 33%
	By CMR: regional RV akinesia or dyskinesia or dyssynchronous RV contraction and 1 of the following: • Ratio of RV end-diastolic volume to BSA $\geq$ 110 mL/m^2 (male) or $\geq$100 mL/m^2 (female) • Or RV ejection fraction $\leq$ 40%
Minor	By RV angiography: regional RV akinesia, dyskinesia, or aneurysm By 2D-TTE: regional RV akinesia or dyskinesia and 1 of the following (end-diastole): • PLAX RVOT $\geq$ 29 to <32 mm (corrected for body size [PLAX/BSA] $\geq$ 16 to <19 mm/m^2) • PSAX RVOT $\geq$ 32 to <36 mm (corrected for body size [PSAX/BSA] $\geq$ 18 to <21 mm/m^2) • Or fractional area change >33% to $\leq$40%
	By CMR: regional RV akinesia or dyskinesia or dyssynchronous RV contraction and 1 of the following • Ratio of RV end-diastolic volume to BSA $\geq$100 to <110 mL/m^2 (male) or $\geq$90 to <100 mL/m^2 (female) • Or RV ejection fraction >40% to $\leq$45%

LV involvement is identified in more than half of patients with ACM, and biventricular as well as predominant LV ACM forms may occur [94], which are associated with a worse prognosis [95]. Specific diagnostic criteria for LV ACM were recently proposed: global LV systolic dysfunction (either LVEF or GLS) with or without LV dilatation, or regional LV hypokinesia/akinesia of the LV free wall or septum are considered minor criteria [93].

Emerging TTE parameters in the evaluation of patients with suspected or established ACM include the measurement of tricuspid annular plane systolic excursion (TAPSE), RV basal diameter, GLS (RV and LV), mechanical dispersion (RV and LV), and the use of 3D

TTE. In particular, RV GLS is affected in early ACM phases [96], TAPSE (as well as fractional area change) are associated with worse outcomes [97], and RV mechanical dispersion correlates with ventricular arrhythmias risk [98]. Besides, LVEF has an incremental prognostic role over RV systolic function [99]. Altogether, an international consensus proposed that prophylactic ICD implantation should be indicated in case of severe RV/LV systolic dysfunction and should be considered if there is moderate RV or LV impairment [100].

Due to the limitations of TTE in RV evaluation, CMR has become an integral part of the diagnostic evaluation in ACM. Beyond determining the presence of morpho-functional ventricular abnormalities, CMR provides information on the presence, morphology, and wall distribution of myocardial fibrofatty scar by LGE or fat-saturation T1 sequences. The same criteria previously described for TTE apply to CMR with corresponding cut-off points and nomograms (Table 7) [92,93]. RVEF by CMR has been incorporated into the risk prediction model of ventricular arrhythmias [101]. The presence of transmural LGE of $\geq$1 RV region or LV LGE of the free wall (subepicardial or intramyocardial) or septum are considered major criteria [93]. Typically, the LGE pattern shows large amounts of contrast uptake in the LV with a non-ischaemic pattern, predominantly involving the subepicardial layers of the inferior and the inferolateral regions (Figure 22). The presence of a subepicardial annular (ring-like pattern) is also suggestive of ACM.

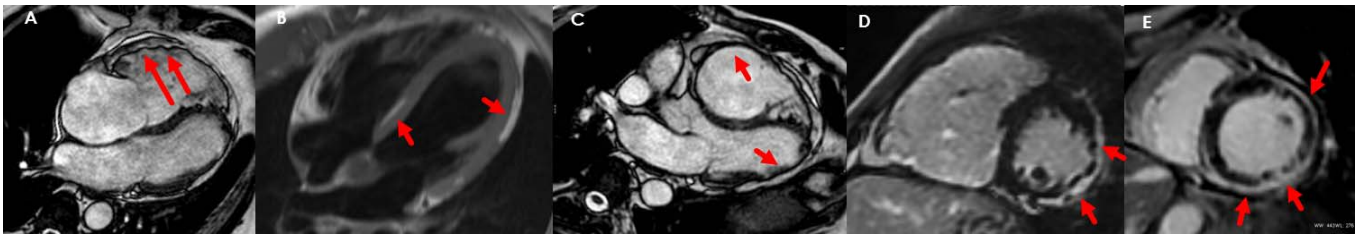

Figure 22. CMR findings in a patient with ACM. (**A**) RV aneurysms (arrows) in cine images. (**B**) Fibrofatty infiltration in T1-weighted turbo spin-echo sequences (arrow). (**C**) Right ventricular enlargement and left ventricular wall thinning (subepicardial fatty infiltration) (arrows) in a 3-chamber view cine. (**D**) Subepicardial LGE (arrows) and (**E**) subepicardial annular (arrows) patterns.

In cases where CMR is contraindicated, CT can be an alternative for the evaluation of RV and LV volumes and EF, aneurysms, fibrofatty infiltration, and wall motion abnormalities. Although generally not used in clinical practice for this purpose, angiography may be an alternative in the evaluation of these patients.

6. Left Ventricular Noncompaction

Left ventricular noncompaction (LVNC) is a heterogeneous entity characterized by prominent LV trabeculae, deep intertrabecular recesses, and a thin compacted (C) myocardial layer [102] (Figure 23). Hypertrabeculation may occur associated with LV dilatation (DCM) or hypertrophy (HCM), and both acquired and genetic LVNC forms may occur.

Different diagnostic criteria have been described for LVNC (Figures 24 and 25). By TTE, the distance from the epicardial surface to the trough of the trabeculae (X) and the distance from the epicardial surface to the peak of the trabeculae (Y) can be measured on short-axis views. A ratio of X/Y $\leq$0.5 at end-diastole is diagnostic of LVNC [103]. Alternatively, a ratio of NC/C layers >2 measured on the short-axis at end-systole is also suggestive of LVNC [104]. By CMR, a ratio of NC/C layers >2.3 measured on long-axis views [105], a trabeculated mass >20% of the total LV mass [106], or a fractal dimension >1.30 [107] are diagnostic of LVNC (all measured at end-diastole). Fulfillment of LVNC morphologic criteria per se has not been associated with LV remodeling [108] or clinical events [109] throughout follow-up. However, the extension of the trabeculae has been recently related to outcomes: patients presenting hypertrabeculation from the apex to the base have been found to have higher mortality [110].

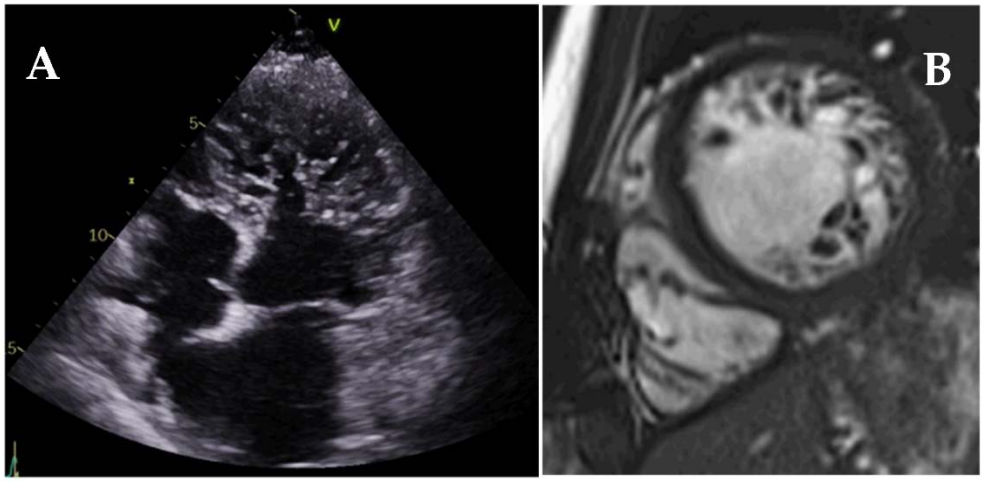

Figure 23. TTE (**A**) and CMR (**B**) images of patients with left ventricular noncompaction showing marked hypertrabeculation and deep intertrabecular recesses.

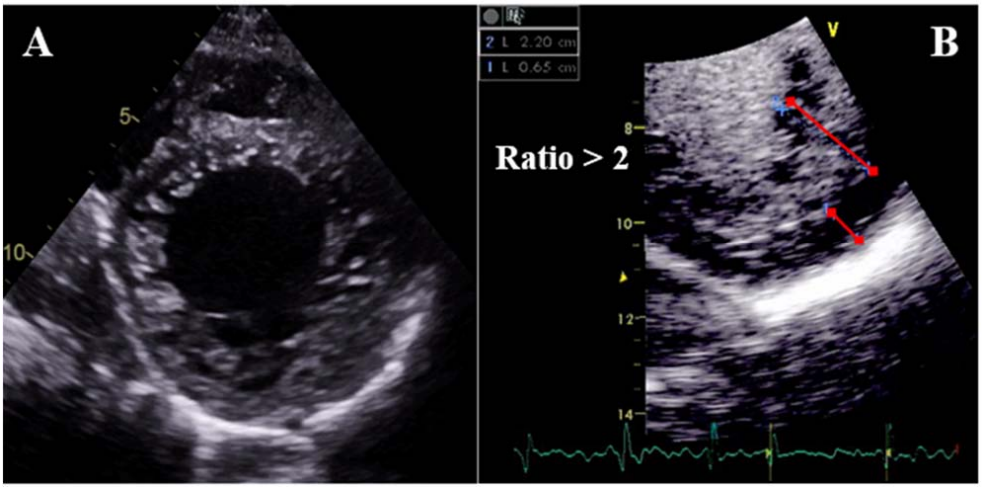

Figure 24. TTE parasternal short-axis mid-ventricular view of a patient with LVNC (**A**). Measurement of the compacted and non-compacted layers at end-diastole after echocontrast administration, fulfilling LVNC diagnostic criteria (**B**).

TTE is the first-line imaging technique for both quantification and localization of the trabeculae: the apex and lateral segments are the most frequently involved. Contrast echocardiography may be used to enhance trabeculation measurement and exclude the presence of intertrabecular thrombi (Figure 24B). Assessment of LVEF is mandatory since it is one of the strongest predictors of outcomes [110–112]. Strain analysis by TTE may detect subclinical myocardial dysfunction [113] and different studies have shown the diagnostic value of strain to differentiate LVNC from healthy controls [113] and DCM [114]. However, no consistent data is available on its prognostic implications.

CMR should be performed in all LVNC patients. The presence of LV dilatation [111,115] and a thinned compacted myocardial layer [115] has been associated with negative outcomes. Although LGE seems to be less frequent in LVNC compared to DCM or HCM [111], and not always related to the most hypertrabeculated segments, it is a powerful and independent predictor of outcomes, with added prognostic implications over LVEF [111,112,116]. Of note, patients with preserved LVEF and negative LGE have an excellent prognosis, while those with positive LGE are at increased risk irrespective of LVEF [116]. LGE has also been associated with SCD risk, even in the absence of severe systolic dysfunction [112]. Mapping techniques have been studied in LVNC; a small report has described worse outcomes with higher ECV values [117]. In addition, feature-tracking strain analysis may be used

to differentiate LVNC from the general population [118] and DCM [119]. However, it is not recommended in routine practice due to lack of standardization and unvalidated association with clinical events.

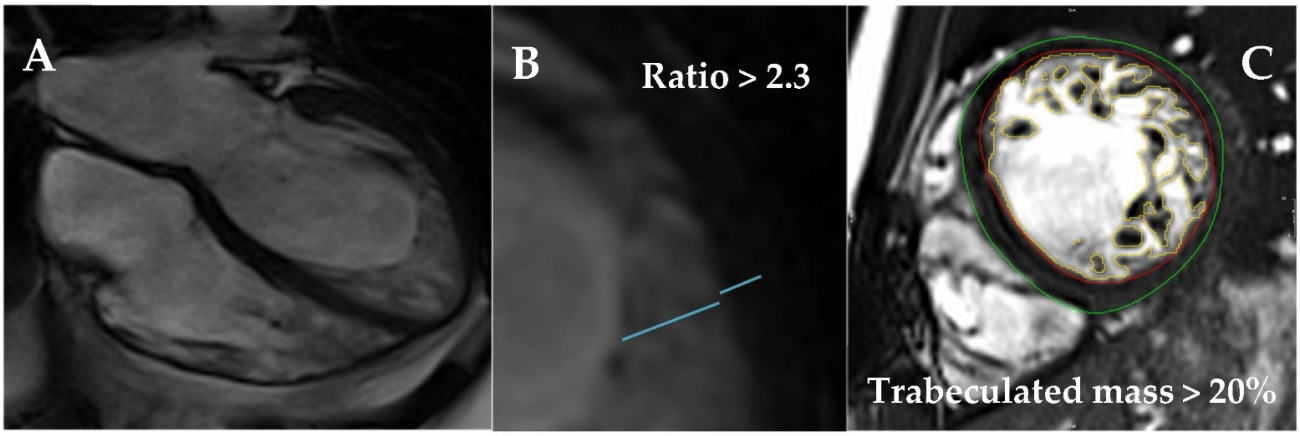

Figure 25. CMR 4-chambers view of a patient with LVNC (**A**). Measurement of the compacted and non-compacted layers at end-diastole on a long-axis view (Petersen criteria, **B**). Measurement of the trabeculated mass on a short-axis view (Jacquier criteria, **C**).

Finally, cardiac CT is rarely used in LVNC, with its main objective being to exclude coronary artery disease. However, a large population study has demonstrated that the degree of hypertrabeculation measured by CT was independently related to outcomes [120]. Therefore, cardiac CT may be considered in patients with contraindications for CMR.

7. Conclusions

Cardiac imaging techniques are an essential tool in the study of cardiomyopathies, and they provide both diagnostic and prognostic relevant information. Transthoracic echocardiography should always be the first technique used due to its availability and cost, as well as the possibility of periodic testing. Cardiovascular magnetic resonance should also be performed in all patients due to its additional anatomical and functional information as well as thorough tissue characterization, with important prognostic implications. Other techniques (e.g., CT, PET-CT, scintigraphy, among others) may be applied in selected entities while more advanced imaging analysis (e.g., strain, myocardial work, mapping, etc.) offer promising but still preliminary results. Altogether, multimodality cardiac imaging plays an important role in clinical decision-making and helps to improve patients' management and outcomes.

Author Contributions: G.C. and J.F.R.-P. have equally contributed to manuscript preparation, writing and revision. All authors have read and agreed to the published version of the manuscript.

Funding: The authors received no financial support for the publication of this article.

Institutional Review Board Statement: Not applicable.

Informed Consent Statement: Not applicable.

Data Availability Statement: See references.

Conflicts of Interest: The authors declare no conflict of interest.

Abbreviations

2D	Two-dimensional
3D	Three-dimensional
ACM	arrhythmogenic cardiomyopathy
AL	primary amyloidosis
ATTR	transthyretin amyloidosis
C/CL	cardiac compared to the contralateral chest
CA	cardiac amyloidosis
CMR	cardiovascular magnetic resonance
CRT	cardiac resynchronization therapy
CS	cardiac sarcoidosis
CT	computed tomography
DCM	dilated cardiomyopathy
ECG	electrocardiogram
ECV	extracellular volume
EMF	endomyocardial fibrosis
ESC	European Society of Cardiology
FD	Anderson–Fabry disease
FDG	18F-fluorodeoxyglucose
GCS	global circumferential strain
GLS	global longitudinal strain
HCM	hypertrophic cardiomyopathy
ICD	implantable cardioverter-defibrillator
IOC	iron overload cardiomyopathy
LGE	late gadolinium enhancement
LV	left ventricle
LVEF	left ventricular ejection fraction
LVH	left ventricular hypertrophy
LVNC	left ventricular noncompaction
LVOTO	left ventricular outflow tract obstruction
MIBG	123I-meta-iodobenzylguanidine
MW	myocardial work
PET	positron emission tomography
RCM	restrictive cardiomyopathies
RV	right ventricle
RVEF	right ventricle ejection fraction
SAM	systolic anterior motion
SCD	sudden cardiac death
TAPSE	tricuspid annular plane systolic excursion
TTE	transthoracic echocardiography

References

1. Elliott, P.; Andersson, B.; Arbustini, E.; Bilinska, Z.; Cecchi, F.; Charron, P.; Dubourg, O.; Kühl, U.; Maisch, B.; McKenna, W.J.; et al. Classification of the cardiomyopathies: A position statement from the european society of cardiology working group on myocardial and pericardial diseases. *Eur. Heart J.* **2008**, *29*, 270–276. [CrossRef]
2. Elliott, P.M.; Anastasakis, A.; Borger, M.A.; Borggrefe, M.; Cecchi, F.; Charron, P.; Hagege, A.A.; Lafont, A.; Limongelli, G.; Mahrholdt, H.; et al. 2014 ESC guidelines on diagnosis and management of hypertrophic cardiomyopathy: The task force for the diagnosis and management of hypertrophic cardiomyopathy of the European Society of Cardiology (ESC). *Eur. Heart J.* **2014**, *35*, 2733–2779. [PubMed]
3. Ommen, S.R.; Mital, S.; Burke, M.A.; Day, S.M.; Deswal, A.; Elliott, P.; Evanovich, L.L.; Hung, J.; Joglar, J.A.; Kantor, P.; et al. 2020 AHA/ACC Guideline for the Diagnosis and Treatment of Patients With Hypertrophic Cardiomyopathy: A Report of the American College of Cardiology/American Heart Association Joint Committee on Clinical Practice Guidelines. *J. Am. Coll. Cardiol.* **2020**, *76*, e159–e240. [PubMed]
4. Cardim, N.; Galderisi, M.; Edvardsen, T.; Plein, S.; Popescu, B.A.; D'Andrea, A.; Bruder, O.; Cosyns, B.; Davin, L.; Donal, E.; et al. Role of multimodality cardiac imaging in the management of patients with hypertrophic cardiomyopathy: An expert consensus of the European Association of Cardiovascular Imaging Endorsed by the Saudi Heart Association. *Eur. Hear. J.-Cardiovasc. Imaging* **2015**, *16*, 280. [CrossRef] [PubMed]

5. Urbano-Moral, J.A.; Gutierrez-Garcia-Moreno, L.; Matabuena-Gomez-Limon, J.; Niella, N.; Maldonado, G.; Valle-Racero, J.I.; Niella, M.; Teixido-Tura, G.; Garcia-Dorado, D.; Ferrazzi, P.; et al. Structural abnormalities in hypertrophic cardiomyopathy beyond left ventricular hypertrophy by multimodality imaging evaluation. *Echocardiography* **2019**, *36*, 1241–1252. [CrossRef]
6. Greulich, S.; Seitz, A.; Herter, D.; Günther, F.; Probst, S.; Bekeredjian, R.; Gawaz, M.; Sechtem, U.; Mahrholdt, H. Long-term risk of sudden cardiac death in hypertrophic cardiomyopathy: A cardiac magnetic resonance outcome study. *Eur. Hear. J. Cardiovasc. Imaging* **2021**, *22*, 732–741. [CrossRef]
7. Harris, K.M.; Spirito, P.; Maron, M.S.; Zenovich, A.G.; Formisano, F.; Lesser, J.R.; Mackey-Bojack, S.; Manning, W.J.; Udelson, J.E.; Maron, B.J. Prevalence, Clinical Profile, and Significance of Left Ventricular Remodeling in the End-Stage Phase of Hypertrophic Cardiomyopathy. *Circulation* **2006**, *114*, 216–225. [CrossRef]
8. O'Mahony, C.; Jichi, F.; Pavlou, M.; Monserrat, L.; Anastasakis, A.; Rapezzi, C.; Biagini, E.; Gimeno, J.R.; Limongelli, G.; McKenna, W.J.; et al. A novel clinical risk prediction model for sudden cardiac death in hypertrophic cardiomyopathy (HCM Risk-SCD). *Eur. Heart J.* **2013**, *35*, 2010–2020. [CrossRef] [PubMed]
9. Tower-Rader, A.; Mohananey, D.; To, A.; Lever, H.M.; Popovic, Z.B.; Desai, M.Y. Prognostic Value of Global Longitudinal Strain in Hypertrophic Cardiomyopathy: A Systematic Review of Existing Literature. *JACC Cardiovasc. Imaging* **2019**, *12*, 1930–1942. [CrossRef] [PubMed]
10. Augusto, J.B.; Davies, R.H.; Bhuva, A.N.; Knott, K.D.; Seraphim, A.; Alfarih, M.; Lau, C.; Hughes, R.K.; Lopes, L.R.; Shiwani, H.; et al. Diagnosis and risk stratification in hypertrophic cardiomyopathy using machine learning wall thickness measurement: A comparison with human test-retest performance. *Lancet Digit. Health* **2021**, *3*, e20–e28. [CrossRef]
11. Chan, R.H.; Maron, B.J.; Olivotto, I.; Pencina, M.J.; Assenza, G.E.; Haas, T.; Lesser, J.R.; Gruner, C.; Crean, A.M.; Rakowski, H.; et al. Prognostic Value of Quantitative Contrast-Enhanced Cardiovascular Magnetic Resonance for the Evaluation of Sudden Death Risk in Patients With Hypertrophic Cardiomyopathy. *Circulation* **2014**, *130*, 484–495. [CrossRef] [PubMed]
12. Mentias, A.; Raeisi-Giglou, P.; Smedira, N.G.; Feng, K.; Sato, K.; Wazni, O.; Kanj, M.; Flamm, S.D.; Thamilarasan, M.; Popovic, Z.B.; et al. Late Gadolinium Enhancement in Patients With Hypertrophic Cardiomyopathy and Preserved Systolic Function. *J. Am. Coll. Cardiol.* **2018**, *72*, 857–870. [CrossRef] [PubMed]
13. Freitas, P.; Ferreira, A.M.; Arteaga-Fernández, E.; Antunes, M.; Mesquita, J.; Abecasis, J.; Marques, H.; Saraiva, C.; Matos, D.N.; Rodrigues, R.; et al. The amount of late gadolinium enhancement outperforms current guideline-recommended criteria in the identification of patients with hypertrophic cardiomyopathy at risk of sudden cardiac death. *J. Cardiovasc. Magn. Reson.* **2019**, *21*, 1–10. [CrossRef] [PubMed]
14. Moon, J.; Reed, E.; Sheppard, M.; Elkington, A.G.; Ho, S.; Burke, M.; Petrou, M.; Pennell, D.J. The histologic basis of late gadolinium enhancement cardiovascular magnetic resonance in hypertrophic cardiomyopathy. *J. Am. Coll. Cardiol.* **2004**, *43*, 2260–2264. [CrossRef] [PubMed]
15. Bruder, O.; Wagner, A.; Jensen, C.J.; Schneider, S.; Ong, P.; Kispert, E.-M.; Nassenstein, K.; Schlosser, T.; Sabin, G.V.; Sechtem, U.; et al. Myocardial Scar Visualized by Cardiovascular Magnetic Resonance Imaging Predicts Major Adverse Events in Patients With Hypertrophic Cardiomyopathy. *J. Am. Coll. Cardiol.* **2010**, *56*, 875–887. [CrossRef]
16. Weng, Z.; Yao, J.; Chan, R.H.; He, J.; Yang, X.; Zhou, Y.; He, Y. Prognostic Value of LGE-CMR in HCM: A Meta-Analysis. *JACC Cardiovasc. Imaging* **2016**, *9*, 1392–1402. [CrossRef]
17. Flett, A.S.; Hasleton, J.; Cook, C.; Hausenloy, D.; Quarta, G.; Ariti, C.; Muthurangu, V.; Moon, J.C. Evaluation of Techniques for the Quantification of Myocardial Scar of Differing Etiology Using Cardiac Magnetic Resonance. *JACC Cardiovasc. Imaging* **2011**, *4*, 150–156. [CrossRef]
18. Raman, B.; Ariga, R.; Spartera, M.; Sivalokanathan, S.; Chan, K.; Dass, S.; Petersen, E.S.; Daniels, M.J.; Francis, J.; Smillie, R.; et al. Progression of myocardial fibrosis in hypertrophic cardiomyopathy: Mechanisms and clinical implications. *Eur. Heart J. Cardiovasc. Imaging* **2019**, *20*, 157–167. [CrossRef]
19. Green, J.J.; Berger, J.S.; Kramer, C.M.; Salerno, M. Prognostic Value of Late Gadolinium Enhancement in Clinical Outcomes for Hypertrophic Cardiomyopathy. *JACC Cardiovasc. Imaging* **2012**, *5*, 370–377. [CrossRef]
20. Dass, S.; Suttie, J.J.; Piechnik, S.K.; Ferreira, V.M.; Holloway, C.J.; Banerjee, R.; Mahmod, M.; Cochlin, L.; Karamitsos, T.D.; Robson, M.D.; et al. Myocardial Tissue Characterization Using Magnetic Resonance Noncontrast T1 Mapping in Hypertrophic and Dilated Cardiomyopathy. *Circ. Cardiovasc. Imaging* **2012**, *5*, 726–733. [CrossRef]
21. Arcari, L.; Hinojar, R.; Engel, J.; Freiwald, T.; Platschek, S.; Zainal, H.; Zhou, H.; Vasquez, M.; Keller, T.; Rolf, A.; et al. Native T1 and T2 provide distinctive signatures in hypertrophic cardiac conditions—Comparison of uremic, hypertensive and hypertrophic cardiomyopathy. *Int. J. Cardiol.* **2020**, *306*, 102–108. [CrossRef]
22. Qin, L.; Min, J.; Chen, C.; Zhu, L.; Gu, S.; Zhou, M.; Yang, W.; Yan, F. Incremental Values of T1 Mapping in the Prediction of Sudden Cardiac Death Risk in Hypertrophic Cardiomyopathy: A Comparison With Two Guidelines. *Front. Cardiovasc. Med.* **2021**, *8*, 661673. [CrossRef]
23. Avanesov, M.; Münch, J.; Weinrich, J.; Well, L.; Säring, D.; Stehning, C.; Tahir, E.; Bohnen, S.; Radunski, U.K.; Muellerleile, K.; et al. Prediction of the estimated 5-year risk of sudden cardiac death and syncope or non-sustained ventricular tachycardia in patients with hypertrophic cardiomyopathy using late gadolinium enhancement and extracellular volume CMR. *Eur. Radiol.* **2017**, *27*, 5136–5145. [CrossRef] [PubMed]

24. Lancellotti, P.; Pellikka, P.A.; Budts, W.; Chaudhry, F.A.; Donal, E.; Dulgheru, R.; Edvardsen, T.; Garbi, M.; Ha, J.-W.; Kane, G.C.; et al. The clinical use of stress echocardiography in non-ischaemic heart disease: Recommendations from the European Association of Cardiovascular Imaging and the American Society of Echocardiography. *Eur. Hear. J.-Cardiovasc. Imaging* **2016**, *17*, 1191–1229. [CrossRef]
25. Smiseth, A.O.; Morris, A.D.; Cardim, N.; Cikes, M.; Delgado, V.; Donal, E.; Flachskampf, A.F.; Galderisi, M.; Gerber, B.L.; Gimelli, A.; et al. Multimodality imaging in patients with heart failure and preserved ejection fraction: An expert consensus document of the European Association of Cardiovascular Imaging. *Eur. Heart J.-Cardiovasc. Imaging* **2021**. [CrossRef]
26. Zhao, L.; Ma, X.; Delano, M.C.; Jiang, T.; Zhang, C.; Liu, Y.; Zhang, Z. Assessment of myocardial fibrosis and coronary arteries in hypertrophic cardiomyopathy using combined arterial and delayed enhanced CT: Comparison with MR and coronary angiography. *Eur. Radiol.* **2012**, *23*, 1034–1043. [CrossRef] [PubMed]
27. Pinto, Y.M.; Elliott, P.M.; Arbustini, E.; Adler, Y.; Anastasakis, A.; Böhm, M.; Duboc, D.; Gimeno, J.; De Groote, P.; Imazio, M.; et al. Proposal for a revised definition of dilated cardiomyopathy, hypokinetic non-dilated cardiomyopathy, and its implications for clinical practice: A position statement of the ESC working group on myocardial and pericardial diseases. *Eur. Heart J.* **2016**, *37*, 1850–1858. [CrossRef] [PubMed]
28. Lang, R.M.; Badano, L.P.; Mor-Avi, V.; Afilalo, J.; Armstrong, A.; Ernande, L.; Flachskampf, F.A.; Foster, E.; Goldstein, S.A.; Kuznetsova, T.; et al. Recommendations for Cardiac Chamber Quantification by Echocardiography in Adults: An Update from the American Society of Echocardiography and the European Association of Cardiovascular Imaging. *Eur. Heart J.-Cardiovasc. Imaging* **2015**, *16*, 233–271. [CrossRef]
29. McDonagh, T.A.; Metra, M.; Adamo, M.; Gardner, R.S.; Baumbach, A.; Böhm, M.; Burri, H.; Butler, J.; Čelutkienė, J.; Chioncel, O.; et al. 2021 ESC Guidelines for the diagnosis and treatment of acute and chronic heart failure. *Eur. Heart J.* **2021**, *42*, 3599–3726. [CrossRef]
30. Yancy, C.W.; Jessup, M.; Bozkurt, B.; Butler, J.; Casey, D.E.; Drazner, M.H.; Fonarow, G.C.; Geraci, S.A.; Horwich, T.; Januzzi, J.L.; et al. 2013 ACCF/AHA guideline for the management of heart failure: A report of the american college of cardiology foundation/american heart association task force on practice guidelines. *Circulation* **2013**, *128*, 240–327. [CrossRef] [PubMed]
31. Cho, G.-Y.; Marwick, T.H.; Kim, H.-S.; Kim, M.-K.; Hong, K.-S.; Oh, D.-J. Global 2-Dimensional Strain as a New Prognosticator in Patients With Heart Failure. *J. Am. Coll. Cardiol.* **2009**, *54*, 618–624. [CrossRef]
32. Russell, K.; Eriksen, M.; Aaberge, L.; Wilhelmsen, N.; Skulstad, H.; Remme, E.W.; Haugaa, K.H.; Opdahl, A.; Fjeld, J.G.; Gjesdal, O.; et al. A novel clinical method for quantification of regional left ventricular pressure–strain loop area: A non-invasive index of myocardial work. *Eur. Heart J.* **2012**, *33*, 724–733. [CrossRef] [PubMed]
33. Wang, C.-L.; Chan, Y.-H.; Wu, V.C.; Lee, H.-F.; Hsiao, F.C.; Chu, P.H. Incremental prognostic value of global myocardial work over ejection fraction and global longitudinal strain in patients with heart failure and reduced ejection fraction. *Eur. Heart J. Cardiovasc. Imaging* **2021**, *22*, 348–356. [CrossRef] [PubMed]
34. Donal, E.; Delgado, V.; Bucciarelli-Ducci, C.; Galli, E.; Haugaa, K.; Charron, P.; Voigt, J.-U.; Cardim, N.; Masci, P.G.; Galderisi, M.; et al. Multimodality imaging in the diagnosis, risk stratification, and management of patients with dilated cardiomyopathies: An expert consensus document from the European Association of Cardiovascular Imaging. *Eur. Heart J.-Cardiovasc. Imaging* **2019**, *20*, 1075–1093. [CrossRef]
35. Assomull, R.G.; Prasad, S.K.; Lyne, J.; Smith, G.; Burman, E.D.; Khan, M.; Sheppard, M.; Poole-Wilson, P.A.; Pennell, D.J. Cardiovascular Magnetic Resonance, Fibrosis, and Prognosis in Dilated Cardiomyopathy. *J. Am. Coll. Cardiol.* **2006**, *48*, 1977–1985. [CrossRef]
36. Wu, K.C.; Weiss, R.G.; Thiemann, D.R.; Kitagawa, K.; Schmidt, A.; Dalal, D.; Lai, S.; Bluemke, D.; Gerstenblith, G.; Marbán, E.; et al. Late Gadolinium Enhancement by Cardiovascular Magnetic Resonance Heralds an Adverse Prognosis in Nonischemic Cardiomyopathy. *J. Am. Coll. Cardiol.* **2008**, *51*, 2414–2421. [CrossRef]
37. Becker, M.; Cornel, J.; van de Ven, P.M.; van Rossum, A.C.; Allaart, C.P.; Germans, T. The Prognostic Value of Late Gadolinium-Enhanced Cardiac Magnetic Resonance Imaging in Nonischemic Dilated Cardiomyopathy. *JACC Cardiovasc. Imaging* **2018**, *11*, 1274–1284. [CrossRef]
38. Di Marco, A.; Anguera, I.; Schmitt, M.; Klem, I.; Neilan, T.G.; White, J.A.; Sramko, M.; Masci, P.G.; Barison, A.; Mckenna, P.; et al. Late Gadolinium Enhancement and the Risk for Ventricular Arrhythmias or Sudden Death in Dilated Cardiomyopathy. *JACC Heart Fail.* **2017**, *5*, 28–38. [CrossRef] [PubMed]
39. Neilan, T.G.; Coelho-Filho, O.; Danik, S.B.; Shah, R.V.; Dodson, J.A.; Verdini, D.J.; Tokuda, M.; Daly, C.; Tedrow, U.B.; Stevenson, W.G.; et al. CMR Quantification of Myocardial Scar Provides Additive Prognostic Information in Nonischemic Cardiomyopathy. *JACC Cardiovasc. Imaging* **2013**, *6*, 944–954. [CrossRef]
40. Halliday, B.P.; Gulati, A.; Ali, A.; Guha, K.; Newsome, S.J.; Arzanauskaite, M.; Vassiliou, V.; Lota, A.S.; Izgi, C.; Tayal, U.; et al. Association Between Midwall Late Gadolinium Enhancement and Sudden Cardiac Death in Patients With Dilated Cardiomyopathy and Mild and Moderate Left Ventricular Systolic Dysfunction. *Circulation* **2017**, *135*, 2106–2115. [CrossRef]
41. Halliday, B.P.; Baksi, A.J.; Gulati, A.; Ali, A.; Newsome, S.; Izgi, C.; Arzanauskaite, M.; Lota, A.; Tayal, U.; Vassiliou, V.; et al. Outcome in Dilated Cardiomyopathy Related to the Extent, Location, and Pattern of Late Gadolinium Enhancement. *JACC Cardiovasc. Imaging* **2019**, *12*, 1645–1655. [CrossRef] [PubMed]

42. Di Marco, A.; Brown, P.F.; Bradley, J.; Nucifora, G.; Claver, E.; de Frutos, F.; Dallaglio, P.D.; Comin-Colet, J.; Anguera, I.; Miller, C.A.; et al. Improved Risk Stratification for Ventricular Arrhythmias and Sudden Death in Patients With Nonischemic Dilated Cardiomyopathy. *J. Am. Coll. Cardiol.* **2021**, *77*, 2890–2905. [CrossRef]
43. Mandawat, A.; Chattranukulchai, P.; Mandawat, A.; Blood, A.J.; Ambati, S.; Hayes, B.; Rehwald, W.; Kim, H.W.; Heitner, J.F.; Shah, D.J.; et al. Progression of Myocardial Fibrosis in Nonischemic DCM and Association with Mortality and Heart Failure Outcomes. *JACC Cardiovasc. Imaging* **2021**, *14*, 1338–1350. [CrossRef]
44. Romano, S.; Judd, R.M.; Kim, R.J.; Kim, H.W.; Klem, I.; Heitner, J.F.; Shah, D.J.; Jue, J.; White, B.E.; Indorkar, R.; et al. Feature-Tracking Global Longitudinal Strain Predicts Death in a Multicenter Population of Patients With Ischemic and Nonischemic Dilated Cardiomyopathy Incremental to Ejection Fraction and Late Gadolinium Enhancement. *JACC Cardiovasc. Imaging* **2018**, *11*, 1419–1429. [CrossRef] [PubMed]
45. Puntmann, V.O.; Carr-White, G.; Jabbour, A.; Yu, C.Y.; Gebker, R.; Kelle, S.; Hinojar, R.; Doltra, A.; Varma, N.; Child, N.; et al. T1-Mapping and Outcome in Nonischemic Cardiomyopathy All-Cause Mortality and Heart Failure. *JACC Cardiovasc. Imaging* **2016**, *9*, 40–50. [CrossRef] [PubMed]
46. Thavendiranathan, P.; Walls, M.; Giri, S.; Verhaert, D.; Rajagopalan, S.; Moore, S.; Simonetti, O.P.; Raman, S.V. Improved Detection of Myocardial Involvement in Acute Inflammatory Cardiomyopathies Using T2 Mapping. *Circ. Cardiovasc. Imaging* **2012**, *5*, 102–110. [CrossRef]
47. Gulati, A.; Ismail, T.F.; Jabbour, A.; Alpendurada, F.; Guha, K.; Ismail, N.A.; Raza, S.; Khwaja, J.; Brown, T.D.; Morarji, K.; et al. The Prevalence and Prognostic Significance of Right Ventricular Systolic Dysfunction in Nonischemic Dilated Cardiomyopathy. *Circulation* **2013**, *128*, 1623–1633. [CrossRef]
48. Merlo, M.; Gobbo, M.; Stolfo, D.; Losurdo, P.; Ramani, F.; Barbati, G.; Pivetta, A.; Di Lenarda, A.; Anzini, M.; Gigli, M.; et al. The Prognostic Impact of the Evolution of RV Function in Idiopathic DCM. *JACC Cardiovasc. Imaging* **2016**, *9*, 1034–1042. [CrossRef] [PubMed]
49. Carluccio, E.; Biagioli, P.; Alunni, G.; Murrone, A.; Zuchi, C.; Coiro, S.; Riccini, C.; Mengoni, A.; D'Antonio, A.; Ambrosio, G. Prognostic value of right ventricular dysfunction in heart failure with reduced ejection fraction: Superiority of longitudinal strain over tricuspid annular plane systolic excursion. *Circ. Cardiovasc. Imaging* **2018**, *11*, e006894. [CrossRef]
50. Rossi, A.; Dini, F.L.; Faggiano, P.; Agricola, E.; Cicoira, M.; Frattini, S.; Simioniuc, A.; Gullace, M.; Ghio, S.; Enriquez-Sarano, M.; et al. Independent prognostic value of functional mitral regurgitation in patients with heart failure. A quantitative analysis of 1256 patients with ischaemic and non-ischaemic dilated cardiomyopathy. *Heart* **2011**, *97*, 1675–1680. [CrossRef]
51. Risum, N.; Tayal, B.; Hansen, T.F.; Bruun, N.E.; Jensen, M.T.; Lauridsen, T.K.; Saba, S.; Kisslo, J.; Gorcsan, J.; Sogaard, P. Identification of Typical Left Bundle Branch Block Contraction by Strain Echocardiography Is Additive to Electrocardiography in Prediction of Long-Term Outcome After Cardiac Resynchronization Therapy. *J. Am. Coll. Cardiol.* **2015**, *66*, 631–641. [CrossRef]
52. Feneon, D.; Behaghel, A.; Bernard, A.; Fournet, M.; Mabo, P.; Daubert, J.-C.; Leclercq, C.; Donal, E. Left atrial function, a new predictor of response to cardiac resynchronization therapy? *Heart Rhythm.* **2015**, *12*, 1800–1806. [CrossRef] [PubMed]
53. Galli, E.; Leclercq, C.; Hubert, A.; Bernard, A.; Smiseth, O.A.; Mabo, P.; Samset, E.; Hernandez, A.; Donal, E. Role ofmyocardial constructive work in the identification of responders to CRT. *Eur. Heart J. Cardiovasc. Imaging.* **2018**, *19*, 1010–1018. [CrossRef]
54. Aalen, J.M.; Donal, E.; Larsen, C.K.; Duchenne, J.; Lederlin, M.; Cvijic, M.; Hubert, A.; Voros, G.; Leclercq, C.; Bogaert, J.; et al. Imaging predictors of response to cardiac resynchronization therapy: Left ventricular work asymmetry by echocardiography and septal viability by cardiac magnetic resonance. *Eur. Heart J.* **2020**, *41*, 3813–3823. [CrossRef] [PubMed]
55. Arora, R.; Ferrick, K.J.; Nakata, T.; Kaplan, R.C.; Rozengarten, M.; Latif, F.; Ng, K.; Marcano, V.; Heller, S.; Fisher, J.D.; et al. I-123 MIBG imaging and heart rate variability analysis to predict the need for an implantable cardioverter defribillator. *J. Nucl. Cardiol.* **2003**, *10*, 121–131. [CrossRef]
56. Lee, H.-J.; Im, D.J.; Youn, J.-C.; Chang, S.; Suh, Y.J.; Hong, Y.; Kim, Y.J.; Hur, J.; Choi, B.W. Assessment of myocardial delayed enhancement with cardiac computed tomography in cardiomyopathies: A prospective comparison with delayed enhancement cardiac magnetic resonance imaging. *Int. J. Cardiovasc. Imaging* **2016**, *33*, 577–584. [CrossRef] [PubMed]
57. Habib, G.; Bucciarelli-Ducci, C.; Caforio, A.L.P.; Cardim, N.; Charron, P.; Cosyns, B.; Dehaene, A.; Derumeaux, G.; Donal, E.; Dweck, M.R.; et al. Multimodality Imaging in Restrictive Cardiomyopathies: An EACVI expert consensus document In collaboration with the "Working Group on myocardial and pericardial diseases" of the European Society of Cardiology Endorsed by The Indian Academy of Echocardiogr. *Eur. Heart J. Cardiovasc. Imaging* **2017**, *18*, 1090–1091. [CrossRef]
58. Anderson, H.N.; Cetta, F.; Driscoll, D.J.; Olson, T.M.; Ackerman, M.J.; Johnson, J.N. Idiopathic Restrictive Cardiomyopathy in Children and Young Adults. *Am. J. Cardiol.* **2018**, *121*, 1266–1270. [CrossRef]
59. González-López, E.; López-Sainz, Á.; Garcia-Pavia, P. Diagnóstico y tratamiento de la amiloidosis cardiaca por transtiretina. Progreso y esperanza. *Rev. Española Cardiol.* **2017**, *70*, 991–1004. [CrossRef]
60. Dorbala, S.; Cuddy, S.; Falk, R.H. How to Image Cardiac Amyloidosis: A Practical Approach. *JACC Cardiovasc. Imaging* **2020**, *13*, 1368–1383. [CrossRef]
61. Barros-Gomes, S.; Williams, B.; Nhola, L.F.; Grogan, M.; Maalouf, J.F.; Dispenzieri, A.; Pellikka, P.A.; Villarraga, H.R. Prognosis of Light Chain Amyloidosis With Preserved LVEF: Added Value of 2D Speckle-Tracking Echocardiography to the Current Prognostic Staging System. *JACC Cardiovasc. Imaging* **2017**, *10*, 398–407.

62. Castaño, A.; Narotsky, D.L.; Hamid, N.; Khalique, O.K.; Morgenstern, R.; DeLuca, A.; Rubin, J.; Chiuzan, C.; Nazif, T.; Vahl, T.; et al. Unveiling transthyretin cardiac amyloidosis and its predictors among elderly patients with severe aortic stenosis undergoing transcatheter aortic valve replacement. *Eur. Heart J.* **2017**, *38*, 2879–2887. [CrossRef]
63. Maurer, M.S.; Bokhari, S.; Damy, T.; Dorbala, S.; Drachman, B.M.; Fontana, M.; Grogan, M.; Kristen, A.V.; Lousada, I.; Nativi-Nicolau, J.; et al. Expert Consensus Recommendations for the Suspicion and Diagnosis of Transthyretin Cardiac Amyloidosis. *Circ. Heart Fail.* **2019**, *12*, e006075. [CrossRef] [PubMed]
64. Khanna, S.; Wen, I.; Bhat, A.; Chen, H.H.L.; Gan, G.C.H.; Pathan, F.; Tan, T.C. The Role of Multi-modality Imaging in the Diagnosis of Cardiac Amyloidosis: A Focused Update. *Front. Cardiovasc. Med.* **2020**, *7*, 590557. [CrossRef] [PubMed]
65. Fontana, M.; Pica, S.; Reant, P.; Abdel-Gadir, A.; Treibel, T.A.; Banypersad, S.M.; Maestrini, V.; Barcella, W.; Rosmini, S.; Bulluck, H.; et al. Prognostic Value of Late Gadolinium Enhancement Cardiovascular Magnetic Resonance in Cardiac Amyloidosis. *Circulation* **2015**, *132*, 1570–1579.
66. Pan, J.A.; Kerwin, M.J.; Salerno, M. Native T1 Mapping, Extracellular Volume Mapping, and Late Gadolinium Enhancement in Cardiac Amyloidosis: A Meta-Analysis. *JACC Cardiovasc. Imaging* **2020**, *13*, 1299–1310. [CrossRef]
67. Martinez-Naharro, A.; Treibel, T.; Abdel-Gadir, A.; Bulluck, H.; Zumbo, G.; Knight, D.S.; Kotecha, T.; Francis, R.; Hutt, D.F.; Rezk, T.; et al. Magnetic Resonance in Transthyretin Cardiac Amyloidosis. *J. Am. Coll. Cardiol.* **2017**, *70*, 466–477. [CrossRef]
68. Brownrigg, J.; Lorenzini, M.; Lumley, M.; Elliott, P. Diagnostic performance of imaging investigations in detecting and differentiating cardiac amyloidosis: A systematic review and meta-analysis. *ESC Heart Fail.* **2019**, *6*, 1041–1051. [CrossRef]
69. Hanna, M.; Ruberg, F.L.; Maurer, M.S.; Dispenzieri, A.; Dorbala, S.; Falk, R.H.; Hoffman, J.; Jaber, W.; Soman, P.; Witteles, R.M.; et al. Cardiac Scintigraphy With Technetium-99m-Labeled Bone-Seeking Tracers for Suspected Amyloidosis. *J. Am. Coll. Cardiol.* **2020**, *75*, 2851–2862. [CrossRef]
70. Hutt, D.F.; Fontana, M.; Burniston, M.; Quigley, A.-M.; Petrie, A.; Ross, J.C.; Page, J.; Martinez-Naharro, A.; Wechalekar, A.D.; Lachmann, H.J.; et al. Prognostic utility of the Perugini grading of 99mTc-DPD scintigraphy in transthyretin (ATTR) amyloidosis and its relationship with skeletal muscle and soft tissue amyloid. *Eur. Heart J. Cardiovasc. Imaging* **2017**, *18*, 1344–1350. [CrossRef]
71. Castano, A.; Haq, M.; Narotsky, D.L.; Goldsmith, J.; Weinberg, R.L.; Morgenstern, R.; Pozniakoff, T.; Ruberg, F.L.; Miller, E.; Berk, J.L.; et al. Multicenter Study of Planar Technetium 99m Pyrophosphate Cardiac Imaging. *JAMA Cardiol.* **2016**, *1*, 880–889. [CrossRef] [PubMed]
72. Sperry, B.W.; Vranian, M.N.; Tower-Rader, A.; Hachamovitch, R.; Hanna, M.; Brunken, R.; Phelan, D.; Cerqueira, M.D.; Jaber, W.A. Regional Variation in Technetium Pyrophosphate Uptake in Transthyretin Cardiac Amyloidosis and Impact on Mortality. *JACC Cardiovasc. Imaging* **2018**, *11*, 234–242. [CrossRef]
73. Deva, D.P.; Hanneman, K.; Li, Q.; Ng, M.Y.; Wasim, S.; Morel, C.; Iwanochko, R.M.; Thavendiranathan, P.; Crean, A.M. Cardiovascular magnetic resonance demonstration of the spectrum of morphological phenotypes and patterns of myocardial scarring in Anderson-Fabry disease. *J. Cardiovasc. Magn. Reson.* **2016**, *18*, 14. [CrossRef]
74. Krämer, J.; Niemann, M.; Liu, D.; Hu, K.; Machann, W.; Beer, M.; Wanner, C.; Ertl, G.; Weidemann, F. Two-dimensional speckle tracking as a non-invasive tool for identification of myocardial fibrosis in Fabry disease. *Eur. Heart J.* **2013**, *34*, 1587–1596. [CrossRef] [PubMed]
75. Moon, J.; Sachdev, B.; Elkington, A.G.; McKenna, W.J.; Mehta, A.; Pennell, D.; Leed, P.J.; Elliott, P. Gadolinium enhanced cardiovascular magnetic resonance in Anderson-Fabry disease Evidence for a disease specific abnormality of the myocardial interstitium. *Eur. Heart J.* **2003**, *24*, 2151–2155. [CrossRef] [PubMed]
76. Biegstraaten, M.; Arngrímsson, R.; Barbey, F.; Boks, L.; Cecchi, F.; Deegan, P.B.; Feldt-Rasmussen, U.; Geberhiwot, T.; Germain, D.P.; Hendriksz, C.; et al. Recommendations for initiation and cessation of enzyme replacement therapy in patients with Fabry disease: The European Fabry Working Group consensus document. *Orphanet, J. Rare Dis.* **2015**, *10*, 36. [CrossRef]
77. Nordin, S.; Kozor, R.; Baig, S.; Abdel-Gadir, A.; Medina-Menacho, K.; Rosmini, S.; Captur, G.; Tchan, M.; Geberhiwot, T.; Murphy, E.; et al. Cardiac Phenotype of Prehypertrophic Fabry Disease. *Circ. Cardiovasc. Imaging* **2018**, *11*, e007168. [CrossRef]
78. Nappi, C.; Altiero, M.; Imbriaco, M.; Nicolai, E.; Giudice, C.A.; Aiello, M.; Diomiaiuti, C.T.; Pisani, A.; Spinelli, L.; Cuocolo, A. First experience of simultaneous PET/MRI for the early detection of cardiac involvement in patients with Anderson-Fabry disease. *Eur. J. Nucl. Med. Mol. Imaging* **2015**, *42*, 1025–1031. [CrossRef]
79. Imbriaco, M.; Pellegrino, T.; Piscopo, V.; Petretta, M.; Ponsiglione, A.; Nappi, C.; Puglia, M.; Dell'Aversana, S.; Riccio, E.; Spinelli, L.; et al. Cardiac sympathetic neuronal damage precedes myocardial fibrosis in patients with Anderson-Fabry disease. *Eur. J. Nucl. Med. Mol. Imaging* **2017**, *44*, 2266–2273. [CrossRef]
80. Gujja, P.; Rosing, D.R.; Tripodi, D.J.; Shizukuda, Y. Iron Overload Cardiomyopathy: Better Understanding of an Increasing Disorder. *J. Am. Coll. Cardiol.* **2010**, *56*, 1001–1012. [CrossRef]
81. Kirk, P.; Roughton, M.; Porter, J.B.; Walker, J.M.; Tanner, M.A.; Patel, J.; Wu, D.; Taylor, J.; Westwood, M.A.; Anderson, L.J.; et al. Cardiac T2* magnetic resonance for prediction of cardiac complications in Thalassemia Major. *Circulation* **2009**, *120*, 1961–1968. [CrossRef] [PubMed]
82. Ghugre, N.R.; Enriquez, C.M.; Gonzalez, I., Jr.; Coates, T.D.; Wood, J.C. MRI detects myocardial iron in the human heart. *Magn. Reson. Med.* **2006**, *56*, 681–686. [CrossRef] [PubMed]
83. Skold, C.M.; Larsen, F.F.; Rasmussen, E.; Pehrsson, S.K.; Eklund, A.G. Determination of cardiac involvement in sarcoidosis by magnetic resonance imaging and Doppler echocardiography. *J. Intern. Med.* **2002**, *252*, 465–471. [CrossRef]

84. Glikson, M.; Nielsen, J.C.; Kronborg, M.B.; Michowitz, Y.; Auricchio, A.; Barbash, I.M.; Barrabés, J.A.; Boriani, G.; Braunschweig, F.; Brignole, M.; et al. 2021 ESC Guidelines on cardiac pacing and cardiac resynchronization therapy. *Eur. Heart J.* **2021**, *42*, 3427–3520. [CrossRef]
85. Vita, T.; Okada, D.R.; Veillet-Chowdhury, M.; Bravo, P.E.; Mullins, E.; Hulten, E.; Agrawal, M.; Madan, R.; Taqueti, V.R.; Steigner, M.; et al. Complementary Value of Cardiac Magnetic Resonance Imaging and Positron Emission Tomography/Computed Tomography in the Assessment of Cardiac Sarcoidosis. *Circ. Cardiovasc. Imaging* **2018**, *11*, e007030. [CrossRef]
86. Youssef, G.; Leung, E.; Mylonas, I.; Nery, P.; Williams, K.; Wisenberg, G.; Gulenchyn, K.Y.; Dekemp, R.A.; DaSilva, J.; Birnie, D.; et al. The Use of 18F-FDG PET in the Diagnosis of Cardiac Sarcoidosis: A Systematic Review and Metaanalysis Including the Ontario Experience. *J. Nucl. Med.* **2012**, *53*, 241–248. [CrossRef]
87. Blankstein, R.; Osborne, M.; Naya, M.; Waller, A.; Kim, C.K.; Murthy, V.; Kazemian, P.; Kwong, R.Y.; Tokuda, M.; Skali, H.; et al. Cardiac Positron Emission Tomography Enhances Prognostic Assessments of Patients With Suspected Cardiac Sarcoidosis. *J. Am. Coll. Cardiol.* **2014**, *63*, 329–336. [CrossRef]
88. Dweck, M.; Abgral, R.; Trivieri, M.G.; Robson, P.M.; Karakatsanis, N.; Mani, V.; Palmisano, A.; Miller, M.A.; Lala, A.; Chang, H.L.; et al. Hybrid Magnetic Resonance Imaging and Positron Emission Tomography With Fluorodeoxyglucose to Diagnose Active Cardiac Sarcoidosis. *JACC Cardiovasc. Imaging* **2018**, *11*, 94–107. [CrossRef]
89. Mocumbi, A.O.; Carrilho, C.; Sarathchandra, P.; Ferreira, M.B.; Yacoub, M.; Burke, M. Echocardiography accurately assesses the pathological abnormalities of chronic endomyocardial fibrosis. *Int. J. Cardiovasc. Imaging* **2010**, *27*, 955–964. [CrossRef] [PubMed]
90. Mocumbi, A.; Ferreira, M.B.; Sidi, D.; Yacoub, M.H. A Population Study of Endomyocardial Fibrosis in a Rural Area of Mozambique. *N. Engl. J. Med.* **2008**, *359*, 43–49. [CrossRef]
91. Salemi, V.M.; Rochitte, C.E.; Shiozaki, A.A.; Andrade, J.M.; Parga, J.R.; de Ávila, L.F.; Benvenuti, L.A.; Cestari, I.N.; Picard, M.H.; Kim, R.J.; et al. Late Gadolinium Enhancement Magnetic Resonance Imaging in the Diagnosis and Prognosis of Endomyocardial Fibrosis Patients. *Circ. Cardiovasc. Imaging* **2011**, *4*, 304–311. [CrossRef]
92. Marcus, F.I.; McKenna, W.J.; Sherrill, D.; Basso, C.; Bauce, B.; Bluemke, D.A.; Calkins, H.; Corrado, D.; Cox, M.G.; Daubert, J.P.; et al. Diagnosis of arrhythmogenic right ventricular cardiomyopathy/dysplasia: Proposed Modification of the Task Force Criteria. *Eur. Heart J.* **2010**, *121*, 1533–1541. [CrossRef]
93. Corrado, D.; Perazzolo Marra, M.; Zorzi, A.; Beffagna, G.; Cipriani, A.; Lazzari, M.; Migliore, F.; Pilichou, K.; Rampazzo, A.; Rigato, I.; et al. Diagnosis of arrhythmogenic cardiomyopathy: The Padua criteria. *Int. J. Cardiol.* **2020**, *319*, 106–114. [CrossRef] [PubMed]
94. Corrado, D.; Basso, C. Arrhythmogenic left ventricular cardiomyopathy. *Heart* **2021**, *120*, 2613–2614. [CrossRef]
95. Aquaro, G.D.; De Luca, A.; Cappelletto, C.; Raimondi, F.; Bianco, F.; Botto, N.; Lesizza, P.; Grigoratos, C.; Minati, M.; Dell'Omodarme, M.; et al. Prognostic Value of Magnetic Resonance Phenotype in Patients With Arrhythmogenic Right Ventricular Cardiomyopathy. *J. Am. Coll. Cardiol.* **2020**, *75*, 2753–2765. [CrossRef] [PubMed]
96. Teske, A.J.; Cox, M.G.; Riele, A.T.; De Boeck, B.W.; Doevendans, P.A.; Hauer, R.N.; Cramer, M.J. Early Detection of Regional Functional Abnormalities in Asymptomatic ARVD/C Gene Carriers. *J. Am. Soc. Echocardiogr.* **2012**, *25*, 997–1006. [CrossRef] [PubMed]
97. Saguner, A.M.; Vecchiati, A.; Baldinger, S.H.; Rüeger, S.; Medeiros-Domingo, A.; Mueller-Burri, A.S.; Haegeli, L.M.; Biaggi, P.; Manka, R.; Lüscher, T.F.; et al. Different prognostic value of functional right ventricular parameters in arrhythmogenic right ventricular cardiomyopathy/dysplasia. *Circ. Cardiovasc. Imaging* **2014**, *7*, 230–239. [CrossRef]
98. Sarvari, S.I.; Haugaa, K.H.; Anfinsen, O.-G.; Leren, T.P.; Smiseth, O.A.; Kongsgaard, E.; Amlie, J.P.; Edvardsen, T. Right ventricular mechanical dispersion is related to malignant arrhythmias: A study of patients with arrhythmogenic right ventricular cardiomyopathy and subclinical right ventricular dysfunction. *Eur. Heart J.* **2011**, *32*, 1089–1096. [CrossRef]
99. Pinamonti, B.; Dragos, A.M.; Pyxaras, S.A.; Merlo, M.; Pivetta, A.; Barbati, G.; Di Lenarda, A.; Morgera, T.; Mestroni, L.; Sinagra, G. Prognostic predictors in arrhythmogenic right ventricular cardiomyopathy: Results from a 10-year registry. *Eur. Heart J.* **2011**, *32*, 1105–1113. [CrossRef] [PubMed]
100. Corrado, D.; Wichter, T.; Link, M.S.; Hauer, R.; Marchlinski, F.; Anastasakis, A. Treatment of arrhythmogenic right ventricular cardiomyopathy/dysplasia: An international task force consensus statement. *Eur. Heart J.* **2015**, *36*, 3227–3237. [CrossRef]
101. Cadrin-Tourigny, J.; Bosman, L.P.; Nozza, A.; Wang, W.; Tadros, R.; Bhonsale, A.; Bourfiss, M.; Fortier, A.; Lie, Ø.H.; Saguner, A.M.; et al. A new prediction model for ventricular arrhythmias in arrhythmogenic right ventricular cardiomyopathy. *Eur. Heart J.* **2019**, *40*, 1850–1858. [CrossRef]
102. Towbin, J.A.; Lorts, A.; Lynn, J. Left ventricular non-compaction cardiomyopathy. *Lancet* **2015**, *22*, 813–825. [CrossRef]
103. Chin, T.K.; Perloff, J.K.; Williams, R.G.; Jue, K.; Mohrmann, R. Isolated noncompaction of left ventricular myocardium. A study of eight cases. *Circulation* **1990**, *82*, 507–513. [CrossRef]
104. Oechslin, E.N.; Attenhofer Jost, C.H.; Rojas, J.R.; Kaufmann, P.A.; Jenni, R. Long-term follow-up of 34 adults with isolated left ventricular noncompaction: A distinct cardiomyopathy with poor prognosis. *J. Am. Coll. Cardiol.* **2000**, *36*, 493–500. [CrossRef]
105. Petersen, S.E.; Selvanayagam, J.B.; Wiesmann, F.; Robson, M.D.; Francis, J.M.; Anderson, R.H.; Watkins, H.; Neubauer, S. Left Ventricular Non-Compaction: Insights From Cardiovascular Magnetic Resonance Imaging. *J. Am. Coll. Cardiol.* **2005**, *46*, 101–105. [CrossRef] [PubMed]

106. Jacquier, A.; Thuny, F.; Jop, B.; Giorgi, R.; Cohen, F.; Gaubert, J.-Y.; Vidal, V.; Bartoli, J.M.; Habib, G.; Moulin, G. Measurement of trabeculated left ventricular mass using cardiac magnetic resonance imaging in the diagnosis of left ventricular non-compaction. *Eur. Heart J.* **2010**, *31*, 1098–1104. [CrossRef] [PubMed]
107. Captur, G.; Muthurangu, V.; Cook, C.; Flett, A.S.; Wilson, R.; Barison, A.; Sado, D.M.; Anderson, S.; McKenna, W.J.; Mohun, T.J.; et al. Quantification of left ventricular trabeculae using fractal analysis. *J. Cardiovasc. Magn. Reson.* **2013**, *15*, 36. [CrossRef] [PubMed]
108. Zemrak, F.; Ahlman, M.A.; Captur, G.; Mohiddin, S.; Kawel-Boehm, N.; Prince, M.; Moon, J.; Hundley, W.G.; Lima, J.A.; Bluemke, D.; et al. The Relationship of Left Ventricular Trabeculation to Ventricular Function and Structure Over a 9.5-Year Follow-Up. *J. Am. Coll. Cardiol.* **2014**, *64*, 1971–1980. [CrossRef]
109. Ivanov, A.; Dabiesingh, D.S.; Bhumireddy, G.P.; Mohamed, A.; Asfour, A.; Briggs, W.M.; Ho, J.; Khan, S.A.; Grossman, A.; Klem, I.; et al. Prevalence and Prognostic Significance of Left Ventricular Noncompaction in Patients Referred for Cardiac Magnetic Resonance Imaging. *Circ. Cardiovasc. Imaging* **2017**, *10*, 1–10. [CrossRef]
110. Vaidya, V.R.; Lyle, M.; Miranda, W.R.; Farwati, M.; Isath, A.; Patlolla, S.H.; Hodge, D.O.; Asirvatham, S.J.; Kapa, S.; Deshmukh, A.J.; et al. Long-Term Survival of Patients With Left Ventricular Noncompaction. *J. Am. Hear. Assoc.* **2021**, *10*, e015563. [CrossRef] [PubMed]
111. Andreini, D.; Pontone, G.; Bogaert, J.; Roghi, A.; Barison, A.; Schwitter, J.; Mushtaq, S.; Vovas, G.; Sormani, P.; Aquaro, G.D.; et al. Long-Term Prognostic Value of Cardiac Magnetic Resonance in Left Ventricle Noncompaction: A Prospective Multicenter Study. *J. Am. Coll. Cardiol.* **2016**, *68*, 2166–2181. [CrossRef]
112. Casas, G.; Limeres, J.; Oristrell, G.; Gutierrez-Garcia, L.; Andreini, D.; Borregan, M.; Larrañaga-Moreira, J.M.; Lopez-Sainz, A.; Codina-Solà, M.; Teixido-Tura, G.; et al. Clinical Risk Prediction in Patients With Left Ventricular Myocardial Noncompaction. *J. Am. Coll. Cardiol.* **2021**, *78*, 643–662. [CrossRef] [PubMed]
113. Bellavia, D.I.; Michelena, H.; Martinez, M.; Pellikka, P.; Bruce, C.J.; Connolly, H.M.; Villarraga, H.R.; Veress, G.; Oh, J.K.; Miller, F. Speckle myocardial imaging modalities for early detection of myocardial impairment in isolated left ventricular non-compaction. *Heart* **2009**, *96*, 440–447. [CrossRef]
114. Tarando, F.; Coisne, D.; Galli, E.; Rousseau, C.; Viera, F.; Bosseau, C.; Habib, G.; Lederlin, M.; Schnell, F.; Donal, E. Left ventricular non-compaction and idiopathic dilated cardiomyopathy: The significant diagnostic value of longitudinal strain. *Int. J. Cardiovasc. Imaging* **2016**, *33*, 83–95. [CrossRef]
115. Ramchand, J.; Podugu, P.; Obuchowski, N.; Harb, S.C.; Chetrit, M.; Milinovich, A.; Griffin, B.; Burrell, L.M.; Tang, W.H.W.; Kwon, D.H.; et al. Novel Approach to Risk Stratification in Left Ventricular Non-Compaction Using A Combined Cardiac Imaging and Plasma Biomarker Approach. *J. Am. Hear. Assoc.* **2021**, *10*, e019209. [CrossRef]
116. Grigoratos, C.; Barison, A.; Ivanov, A.; Andreini, D.; Amzulescu, M.S.; Mazurkiewicz, L.; De Luca, A.; Grzybowski, J.; Masci, P.G.; Marczak, M.; et al. Meta-Analysis of the Prognostic Role of Late Gadolinium Enhancement and Global Systolic Impairment in Left Ventricular Noncompaction. *JACC Cardiovasc. Imaging* **2019**, *12*, 2141–2151. [CrossRef]
117. Araujo-Filho, J.A.B.; Assuncao, A.N.; De Melo, M.D.T.; Bière, L.; Lima, C.R.; Dantas, R.N.; Nomura, C.H.; Salemi, V.M.C.; Jerosch-Herold, M.; Parga, J. Myocardial T1 mapping and extracellular volume quantification in patients with left ventricular non-compaction cardiomyopathy. *Eur. Hear. J.-Cardiovasc. Imaging* **2018**, *19*, 888–895. [CrossRef] [PubMed]
118. Dreisbach, J.G.; Mathur, S.; Houbois, C.P.; Oechslin, E.; Ross, H.; Hanneman, K.; Wintersperger, B.J. Cardiovascular magnetic resonance based diagnosis of left ventricular non-compaction cardiomyopathy: Impact of cine bSSFP strain analysis. *J. Cardiovasc. Magn. Reson.* **2020**, *22*, 9. [CrossRef]
119. Zheng, T.; Ma, X.; Li, S.; Ueda, T.; Wang, Z.; Lu, A.; Zhou, W.; Zou, H.; Zhao, L.; Gong, L. Value of Cardiac Magnetic Resonance Fractal Analysis Combined With Myocardial Strain in Discriminating Isolated Left Ventricular Noncompaction and Dilated Cardiomyopathy. *J. Magn. Reson. Imaging* **2019**, *50*, 153–163. [CrossRef]
120. Sigvardsen, E.P.; Fuchs, A.; Kühl, J.T.; Afzal, S.; Køber, L.; Nordestgaard, B.G.; Kofoed, K.F. Left ventricular trabeculation and major adverse cardiovascular events: The Copenhagen General Population Study. *Eur. Hear. J.-Cardiovasc. Imaging* **2021**, *22*, 67–74. [CrossRef] [PubMed]